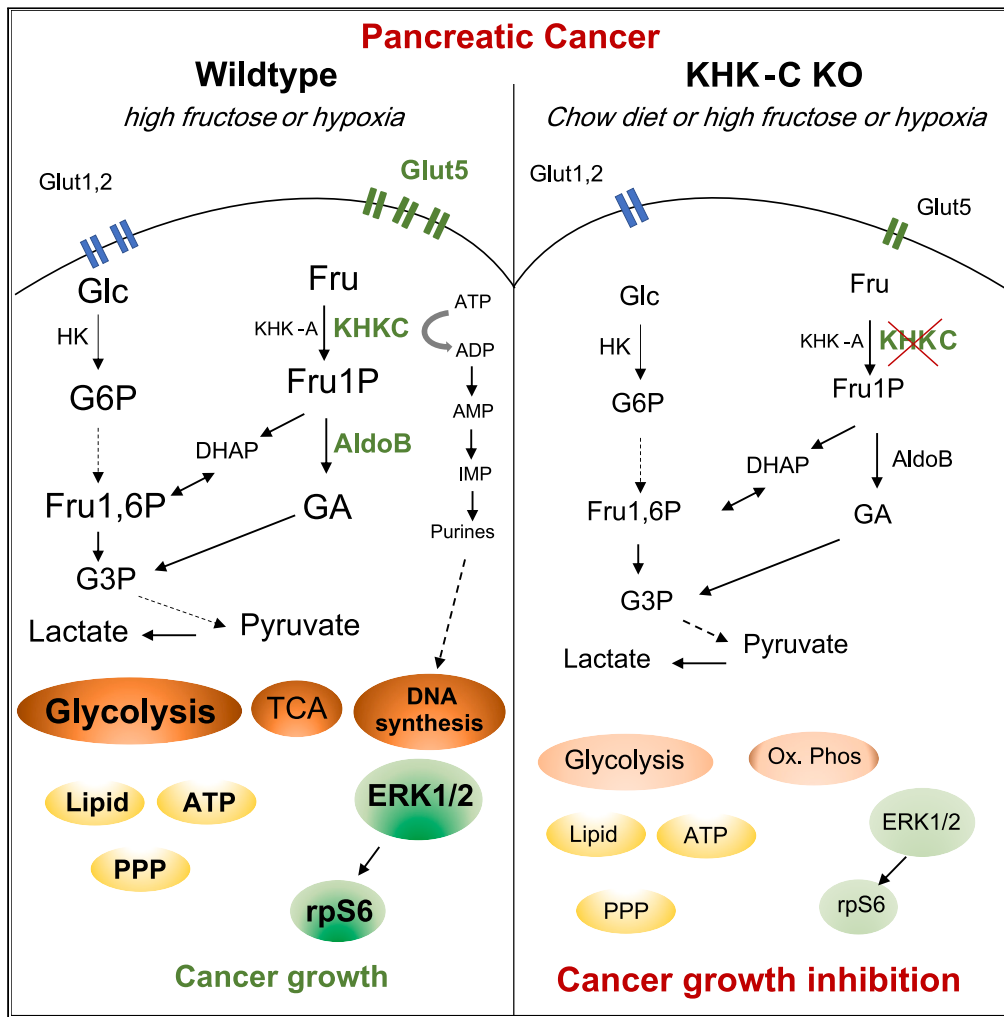


Article

Genetic ablation of ketohexokinase C isoform impairs pancreatic cancer development



Ilaria Guccini,
Guanghai Tang,
Trang Thuy To, ...,
Andrea Alimonti,
Gerald Schwank,
Markus Stoffel

stoffel@biol.ethz.ch

Highlights

Fructose enhances proliferation and decreases the survival of mice with PDAC

KHKC overexpression promotes pancreatic tumor growth

Pancreatic ablation of *KhkC* dampens the proliferation of KPC driven tumors

Pancreatic *KhkC* inactivation rewires PDAC metabolism-related pathways

Guccini et al., iScience 26, 107368
August 18, 2023 © 2023 The Authors.
<https://doi.org/10.1016/j.isci.2023.107368>



Article

Genetic ablation of ketohexokinase C isoform impairs pancreatic cancer development

Ilaria Guccini,¹ Guanghui Tang,¹ Trang Thuy To,¹ Laura Di Rito,² Solange Le Blanc,^{3,10} Oliver Strobel,^{3,10} Mariantonietta D'Ambrosio,^{4,5} Emiliano Pasquini,^{4,5} Marco Bolis,^{4,6} Pamuditha Silva,¹ Hasan Ali Kabakci,¹ Svenja Godbersen,¹ Andrea Alimonti,^{4,5,7,8} Gerald Schwank,^{1,9} and Markus Stoffel^{1,11,*}

SUMMARY

Although dietary fructose is associated with an elevated risk for pancreatic cancer, the underlying mechanisms remain elusive. Here, we report that ketohexokinase (KHK), the rate-limiting enzyme of fructose metabolism, is a driver of PDAC development. We demonstrate that fructose triggers KHK and induces fructolytic gene expression in mouse and human PDAC. Genetic inactivation of *KhkC* enhances the survival of *KPC*-driven PDAC even in the absence of high fructose diet. Furthermore, it decreases the viability, migratory capability, and growth of *KPC* cells in a cell autonomous manner. Mechanistically, we demonstrate that genetic ablation of KHK strongly impairs the activation of KRAS-MAPK pathway and of *rpS6*, a downstream target of mTORC signaling. Moreover, overexpression of KHK in *KPC* cells enhances the downstream KRAS pathway and cell viability. Our data provide new insights into the role of KHK in PDAC progression and imply that inhibiting KHK could have profound implications for pancreatic cancer therapy.

INTRODUCTION

Pancreatic ductal adenocarcinoma (PDAC) is an aggressive tumor and has one of the poorest outcomes, as it is often diagnosed at an advanced stage due to the lack of symptoms. It is projected to be the second leading cause of cancer death by 2030, with the lowest 5-year survival rate of all cancers.^{1,2} At the genetic level, around 80% of patients carry an oncogenic *KRAS* mutation at an early stage of tumor development, followed by loss of function mutations in the tumor suppressors *TP53*, *SMAD4*, and *CDKN2A* (between 90% and 50%) leading to PDAC.³

PDAC tumors display a marked metabolic phenotype and acquire metabolic plasticity to improve cellular fitness to provide a selective advantage for cancer cells during tumorigenesis.^{4,5} Constitutive activation of *KRAS* plays a key role in metabolic reprogramming, in particular, the glycolytic switch to support the synthesis of tumor biomass.⁶ Thus, understanding how metabolism is reprogrammed in pancreatic cancer may provide a strategy for innovative interventional therapies. Carbohydrates serve as energy source for production of building blocks through enhanced glycolysis that sustain uncontrolled proliferation of cancer cells. The intake of dietary sugar has increased dramatically in the Western world during the past four decades and has been paralleled by an increased prevalence for diabetes, obesity, cardiovascular disease, and cancer, implying a possible causal relationship.^{7–11} However, the contribution of specific carbohydrates to disease states is not fully understood. Fructose and glucose are major components of dietary carbohydrates such as sucrose (containing 50% glucose and 50% fructose) and high fructose corn syrup (HFCS, containing 55% fructose and 42% glucose). Glucose can be used directly by various tissues as an energy source or, when in excess, stored in the liver as glycogen or converted into fructose by the polyol pathway.¹² Low doses of fructose are primarily cleared by the liver (90%),^{10,13} while high doses of fructose (≥ 1 g/kg) overwhelm intestinal fructose absorption and clearance, resulting in fructose reaching both the liver and colon, where it can affect gut microbiota and lead to the deterioration of intestinal barrier function.^{14–16} This in turn can cause endotoxemia, inflammation in the liver, and induction of *de novo* lipogenesis.¹⁷ The main difference between glucose and fructose metabolism is that glycolysis is tightly regulated according to the cellular energy state at the level of phosphofructokinase (PFK), while fructose degradation to triosephosphates is unrestricted.¹⁸ The lack of inhibitory feedback mechanisms promotes efficient conversion of fructose into fat. In addition, by limiting ATP levels and restricting ATP-mediated negative

¹Institute of Molecular Health Sciences, ETH Zurich, 8093 Zurich, Switzerland

²Computational Oncology Unit, Department of Oncology, Istituto di Ricerche Farmacologiche 'Mario Negri' IRCCS, 20156 Milano, Italy

³European Pancreas Center, Department of General Surgery, Heidelberg University Hospital, Heidelberg, Germany

⁴Institute of Oncology Research (IOR), Oncology Institute of Southern Switzerland (IOSI), 6500 Bellinzona, Switzerland

⁵Universita' della Svizzera Italiana, 6900 Lugano, Switzerland

⁶Bioinformatics Core Unit, Swiss Institute of Bioinformatics, TI, 6500 Bellinzona, Switzerland

⁷Department of Medicine, University of Padua, 35128 Padua, Italy

⁸Department of Health Sciences and Technology (D-HEST) ETH Zurich, 8093 Zurich, Switzerland

⁹Institute of Pharmacology and Toxicology, University of Zurich, 8057 Zurich, Switzerland

¹⁰Present address: Division of Visceral Surgery, Department of General Surgery, Medical University of Vienna, Vienna, Austria

¹¹Lead contact

*Correspondence: stoffel@biol.ethz.ch

<https://doi.org/10.1016/j.isci.2023.107368>



feedback inhibition of PFK, unrestrained KHK-driven phosphorylation of fructose can also facilitate high glycolytic flux.¹⁹ Ketohexokinase (KHK) is the rate-limiting first enzyme of fructose metabolism that converts fructose to fructose-1-phosphate (F1P), which is then further metabolized by aldolase B to enter glycolysis.²⁰ KHK exists as a high affinity KHK-C and a low affinity KHK-A isoform that are generated by mutually exclusive splicing of exons 3C and 3A, respectively, of the *KHK* gene.²¹ Alternative splicing of *KhkC* in the liver is mediated by APOBEC1 complementation factor (A1CF), while heterogeneous nuclear ribonucleoprotein H1/2 (hnRNP1/2) mediates a c-myc-driven switch of KHKC to the KHKA isoform in dedifferentiated hepatocellular carcinoma (HCC) cells.^{16,22}

Recent studies have shown that fructose consumption is linked to many different types of cancers. Increased fructose uptake, through GLUT5 upregulation, contributes to reinforcing glycolysis in human colorectal, breast, lung cancer, and glioma as well as pancreatic cancer, triggering cell survival and proliferation.^{12,23} In intestinal cancer, a daily small dose of high-fructose corn syrup enhanced tumor growth in adenomatous polyposis coli (APC)-mutant mice, independent of obesity or metabolic syndrome.²⁴ Similarly in acute myeloid leukemia and in prostate cancer, fructose uptake increased cancer cell proliferation and migration *in vitro* and tumor growth *in vivo*.^{25–27} Loss of KHK function is associated with neoplastic disease, as lower KHK transcript levels or reduced KHK enzymatic activity has been reported in most cancers. However, studies investigating the cell autonomous impact of different KHK-isoforms on cancer cells in connection with fructose metabolism are lacking.

In this study, we dissected the role of different KHK isoforms and fructose metabolism in the development and progression of pancreatic cancer. We demonstrate that KHK is upregulated in pancreatic cancer and show that genetic ablation of *KHKC* is sufficient to delay the onset and the development of PDAC *KPC*-driven PDAC *in vivo* by downregulating MAPK and mTOR signaling. Genetic ablation of the *KHKA* isoform in turn triggers a reprogrammed transcriptional and metabolic profile that confers higher proliferation than *KPC;KhkC^{-/-}*, *KPC;KhkA/C^{-/-}* as well as *KPC* PDAC tumors. Importantly, we show that blocking KHK efficiently prevents the proliferation and the growth of PDAC tumors independently of a high fructose diet.

RESULTS

Ketohexokinase is upregulated in murine and human PDAC

To determine the relevance of KHK in the exocrine pancreas, we first analyzed the protein levels and compared its expression to organs with known fructose metabolizing function. KHK was highly expressed in the mouse liver and kidney, consistent with the known high fructokinase activity in these organs, while KHK levels in the pancreas were profoundly lower than in the liver and kidney (Figure S1A). To explore the expression and function of KHK in PDAC development, we took advantage of a conditional mouse PDAC model that is based on the exocrine pancreas-specific activation of *Kras^{G12D}* and loss of *Trp53* and instigated by *Ptf1α-Cre* recombination (*Ptf1α-Cre; LSL-KRAS^{G12D}; Trp53^{fl/+}*, hereafter termed *KPC*).^{28–30} Interestingly, we measured higher KHK expression in pancreatic tumor biopsies compared to the normal controls (*LSL-KRAS^{G12D}; Trp53^{fl/+}*, *KP*) (Figures 1A and 1B). KHK enzymatic activity was also increased (Figure 1C), which likely can be attributed to the upregulation of the KHKC isoform, while the KHKA isoform was not (Figure S1B). Furthermore, we saw a robust upregulation of GLUT5 and ALDOB, and increased phosphorylation of pERK and pAKT (Figure S1B).

We next generated epithelial tumor organoids of *KP* and *KPC* pancreata. This *in vitro* model fully recapitulated the ductal cell lineage characteristics as shown by high *Ck19* and *Sox9* that were enriched in the *KP* and *KPC* organoids compared to the total pancreatic tissue. Genes associated with the acinar (*Ptf1α*, *Cpa1*, and *Amy*), and endocrine (*Ngn3*, *Chga*, and *Ins2*) lineages were not expressed in either *KP* or *KPC* organoids (Figure S1C). In addition, *KPC* organoids upregulated genes that are indicative of a PanIN disease state (*Muc5ac*, *Muc6*, and *Tff1*) in comparison to *KP* (Figure S1D).³¹ Consistent with the observations in mouse tumors, epithelial *KPC* tumor organoids exhibited higher GLUT5, KHK, ALDOB protein levels, and higher activity of KHK compared to the normal *KP* organoids. In addition, we measured increased levels of glycolytic (*Slc2A1* and *Hk2*) and fructolytic transcripts (*Slc2A5*, *KhkA/C*, and *AldoB*) (Figures 1D–1F).

To determine the expression of KHK in biopsies of patients with pancreatic carcinoma we performed immunohistochemical analysis (IHC) of tissue sections of human tumor and adjacent non-tumor pancreatic tissues in 42 cases. While the majority of tumor tissues stained positive for KHK, the adjacent non-tumor pancreatic tissues displayed low or no positivity (Figures 1G and 1H). Interestingly, patient-derived organoids (PDO) from pancreatic cancer showed overexpression of key glycolytic and fructolytic transcripts upon

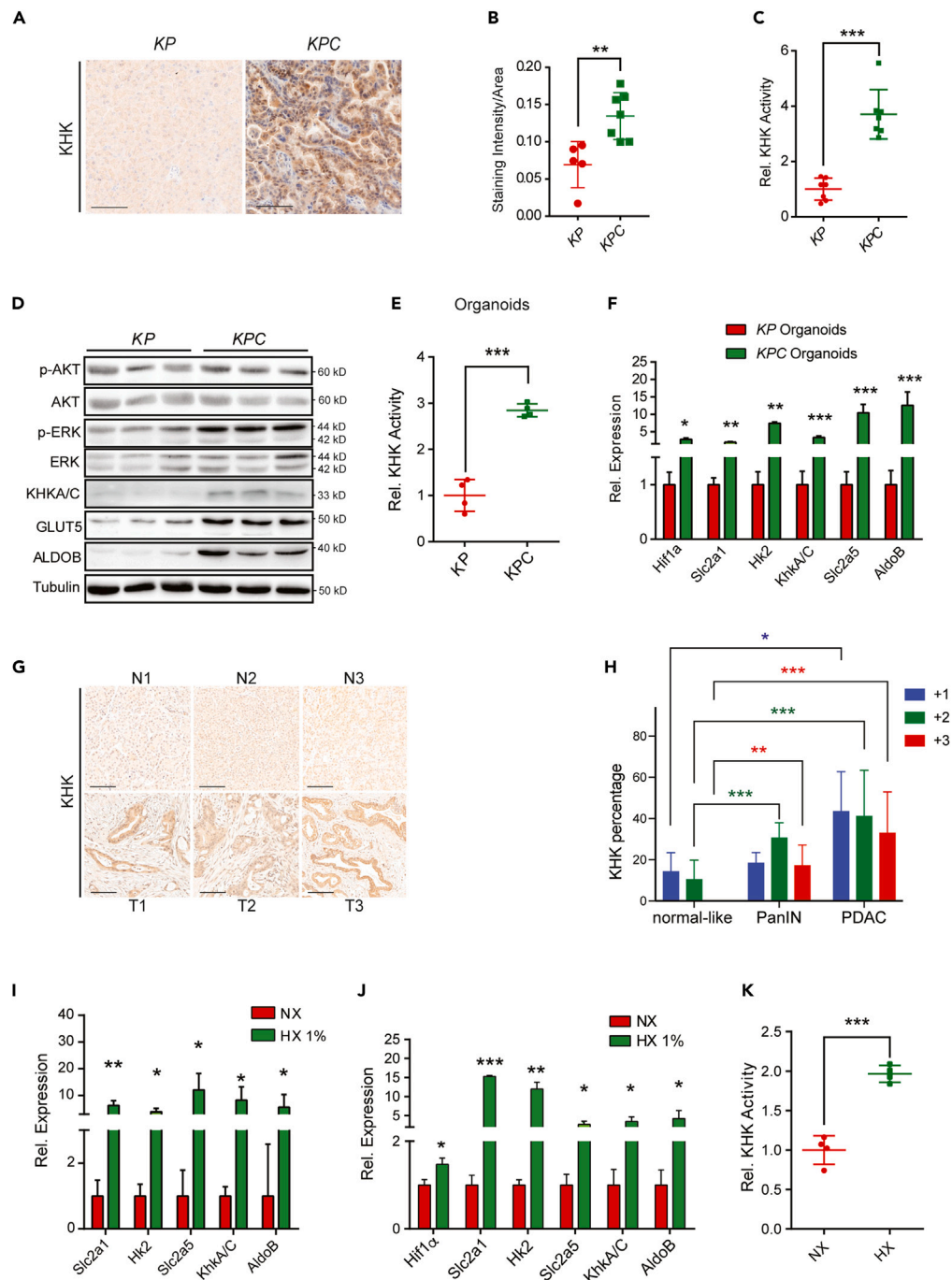


Figure 1. KHK/A/C is overexpressed in human and mouse PDAC tumors

(A) Representative images of KHK in KP versus KPC mouse pancreata at the age of 20 weeks. Scale bar: 100 μ m.
 (B) Quantification, represented as mean of staining intensity/area of KHK from KP versus KPC mouse pancreata, n = 13.
 (C) KHK activity measured in mouse pancreata, n = 7.
 (D) Western blots of indicated proteins from KP versus KPC mouse tumor organoids. Each lane represents an independent tumor organoid.
 (E) KHK activity determined in KP and KPC organoids, n = 4.
 (F) Expression levels of glycolytic and fructose metabolism genes in KP and KPC mouse organoids, n = 3.
 (G) Representative IHC images of KHK in human normal pancreata and PDAC tumors. Scale bar: 100 μ m.
 (H) KHK staining intensities as a percentage per area determined by IHC stainings, n = 42.
 (I) Relative expression of KHK/A/C and related genes in NX and HX 1% groups.
 (J) Relative expression of KHK/A/C and related genes in NX and HX 1% groups.
 (K) Relative KHK activity in NX and HX groups.

Figure 1. Continued

(I) Transcript levels of glycolytic and fructose metabolism genes in human *KPC* organoids in normoxic and hypoxic (1%) conditions, $n = 3$.

(J) Relative transcript levels of glycolytic and fructose metabolism genes in *KPC* organoids, cultured in normoxic and hypoxic (1%) conditions for 24 h, $n = 3$.

(K) KHK activity of *KPC* organoids cultured in normoxic and hypoxic conditions for 24 h, $n = 4$. Data are represented as Mean \pm SEM. The p values were determined by Student's t test (unpaired two-tailed), n.s. (non-significant), * $p < 0.05$, ** $p < 0.01$ and *** $p < 0.001$.

induction of hypoxia (1%) (Figure 1I). Similarly, key glycolytic and fructolytic transcripts were upregulated, and KHK enzymatic activity was increased in organoids of *KPC* mice upon exposure to hypoxic conditions (Figures 1J and 1K). Together, these data demonstrate that expression of rate-limiting glucose and fructose metabolism genes, including KHK-C, are induced in hypoxic conditions as well as *Kras/p53*-driven pancreatic cancers of mice and humans.

High fructose enhances proliferation and decreases the overall survival of mice with *KPC*-driven PDAC

To investigate the function of KHK and fructose diet in pancreatic cancer development, we first treated mouse-derived organoids with either high (17.3 mM) or low (3 mM) glucose, or low glucose plus high fructose (1 mM). Similar to high glucose, high-fructose treatment enhanced cell proliferation and viability in *KPC* organoids (Figures 2A–2C). Cell viability and growth correlated in a fructose dose-dependent manner in *KPC* compared to control organoids from *KP* mice (Figures S2A and S2B). Interestingly, high fructose treatment (LG + FR) in *KPC* organoids induced the expression of *Slc2a5* and *KhkC*, two rate-limiting proteins for fructose transport into cells and fructose metabolism, while *KhkA* expression was repressed compared to low glucose (LG) treatment. KHK activity was enhanced in high fructose treatment compared to low glucose (Figures 2D and 2E). Consistent with the *in vitro* data, high-fructose diet in mice (25% in drinking water) enhanced KHK expression, the weight and proliferation rates of PDAC tumors as shown by Ki67-positive cells staining (Figures 2F–2H). Strikingly, a high-fructose diet decreased the overall survival of *KPC*, but not of *KP* mice (Figure 2I). Furthermore, we measured higher plasma fructose levels in both *KP* and *KPC* mice treated with a high fructose diet (Figure S2C). Tumors from mice treated with high fructose revealed higher *KhkC* expression but similar *KhkA* levels. Furthermore, *Slc2a5* and *AldoB* transcripts were strongly upregulated upon high dietary fructose exposure (Figure 2J). Similar results were observed in the *KPC* PDAC model harboring the gain-of-function mutation on *Trp53*^{R172H} (hereafter termed *KPC*^{mut}). When exposed to high fructose, these mice, similar to *KPC* animals, exhibited decreased overall survival associated with increased pancreatic tumor burden and higher tumor weight compared to normal diet (Figures S2D–S2I). These results highlight the role of dietary fructose in fructose metabolism, cell proliferation, tumor progression and overall survival in pancreatic cancer *KPC* mice.

KHKC overexpression promotes tumor growth and *KhkC* KO is sufficient to delay the onset and development of tumors

To study the relevance of the different KHK isoforms in our PDAC model systems, we first genetically manipulated *KPC*-derived mouse cells with stable *KhkC* or *KhkA* overexpression or shRNA knockdown of *KhkC* and *KhkA* isoforms, respectively (Figures S3A and S3B). Interestingly, KHKC overexpression increased the cell viability of *KPC* cells, an observation that was even more profound upon high fructose treatment for 48h. On the contrary, *KhkC* knockdown reduced the cell viability of *KPC* cells to similar extent as the complete *KhkA/C* knockdown. *KhkA* overexpression or knockdown did not have any significant impact of *KPC* viability (Figure 3A). When *KPC* cells overexpressing the *KhkC* isoform were treated with [¹⁴C (U)] D-fructose in the medium they displayed higher ¹⁴C incorporation into protein and DNA compared to *KhkA* overexpressing cells. On the contrary, knockdown of *KhkC* impaired ¹⁴C D-fructose incorporation into protein and DNA (Figures 3B and 3C). Of note, analysis of *KhkC* overexpressing cells revealed enhanced activation of the MAPK pathway as shown by increased phosphorylation of ERK (pERK^{Thr202/Tyr204}) and higher levels of ALDOB, while no difference in pERK was measured compared to the control. However, gain of KHK-A function resulted in a strong down-regulation of the RPS6 phosphorylation that is known to correlate with decreased cell proliferation (Figure S3A).^{32,33} To study the impact of KHK isoforms in PDAC onset and development *in vivo* we generated conditional mouse models with specific *KhkA* and *KhkC* ablation, by flanking exons 3a and 3c, respectively, with floxP sites (Figures S3C and S3D). Similar to the *KhkA/C* total knock out mice, *KhkC* and *KhkA* floxed mice crossed with *p48-Cre* were viable and did not show any major pancreatic phenotype compared to C57BL/6

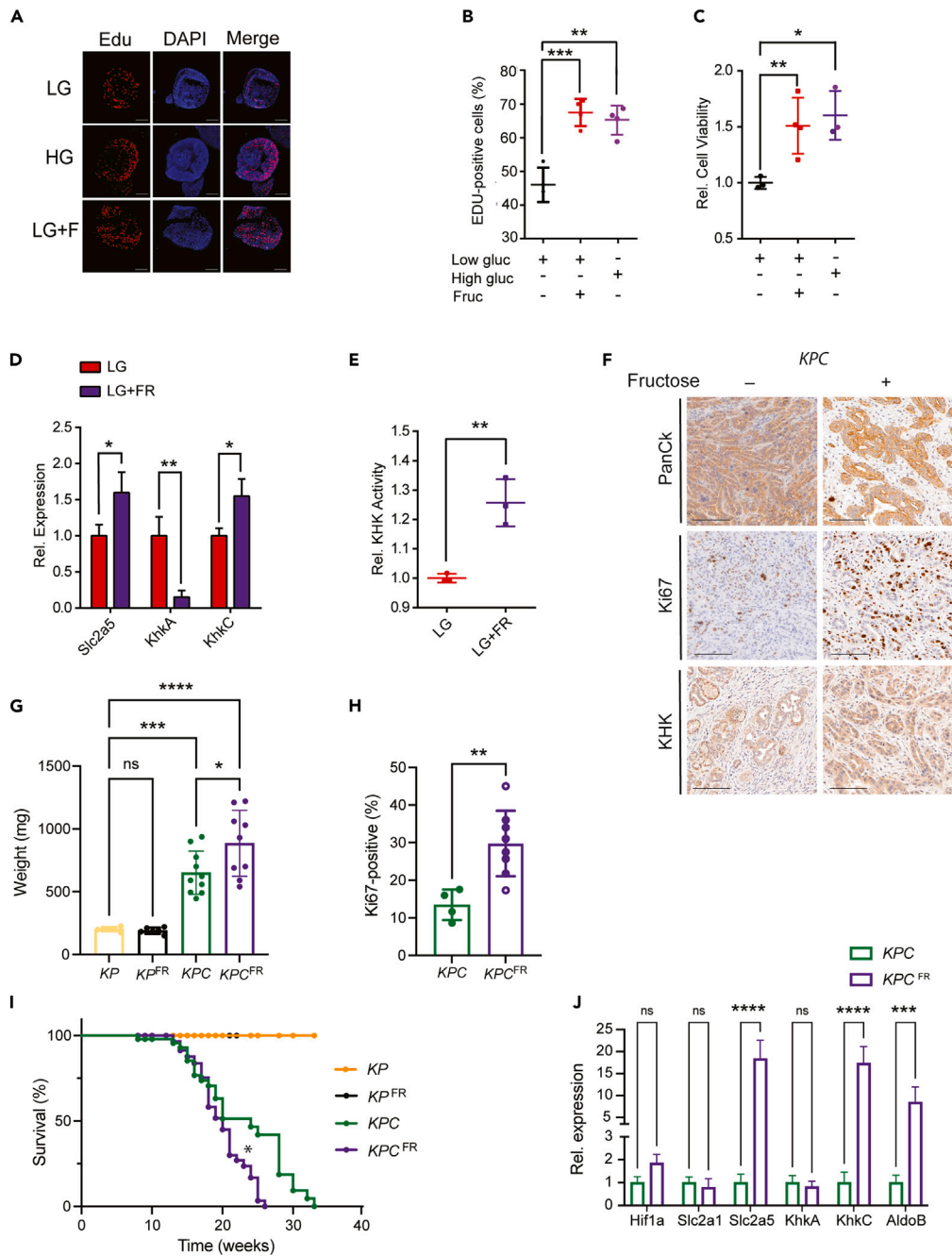


Figure 2. High Fructose enhances proliferation and decreases the overall survival of mice with KPC-driven PDAC

(A) Representative images of Edu incorporation assay performed in KPC organoids and cultured in low glucose (LG, 3 mM), high glucose (HG, 17.3 mM) or low glucose with fructose (LG, 3 mM, 1 mM FR) medium for 48 h. Scale bar: 100 μ m. (B) Dot plot representing the percentage of Edu positive cells from organoids as shown in A, n = 3. (C) Dot plot representing the percentage of cell viability from organoids as shown in A, n = 3. (D) Relative transcript levels of Slc2a5, KhkA and KhkC isoforms in KPC organoids, cultured in low glucose (LG) and low glucose with 1 mM fructose (LG + FR), n = 3. (E) KHK activity measurements of KPC organoids cultured in low glucose (LG) and low glucose with 1 mM fructose (LG + FR), n = 3. (F) Representative IHC images of PanCk (Pan-Cytokeratin), Ki67 and KHK stainings in tissue sections from KPC mice treated with 25% of fructose for 10 weeks. Scale bar: 100 μ m. (G) Organoid weight measurements of KPC organoids cultured in low glucose (LG) and low glucose with 1 mM fructose (LG + FR), n = 3. (H) Ki67-positive cells measurements of KPC organoids cultured in low glucose (LG) and low glucose with 1 mM fructose (LG + FR), n = 3. (I) Survival curve of mice with KPC-driven PDAC treated with 25% of fructose for 10 weeks. (J) Relative expression of Hif1a, Slc2a1, Slc2a5, KhkA, KhkC and AldoB in KPC organoids cultured in low glucose (LG) and low glucose with 1 mM fructose (LG + FR), n = 3.

Figure 2. Continued

- (G) Tumors weight endpoints (mg) from *KP* and *KPC* mice treated with 25% of fructose diet for 10 weeks, $n = 31$ in total. The p values were determined by ANOVA multiple comparison test (Sidák's multiple comparison test).
- (H) Percentage of Ki67 positivity in *KPC* mice treated with 25% of fructose diet for 10 weeks, $n = 12$ in total. The p values were determined by Student's t test (unpaired two-tailed).
- (I) Survival percentage of *KP* and *KPC* mice with or without 25% of fructose diet for 10 weeks. Kaplan-Meier survival curves were compared by Mantel-Cox log rank test, $n = 177$ in total.
- (J) Relative transcript levels of glycolytic (*Hif1 α* , *Slc2a1*) and fructose metabolic genes (*Slc2a5*, *KhkA*, *KhkC* and *AldoB*) in *KPC* pancreata treated with a fructose 25% diet, $n = 3$. Data are represented as Mean \pm SEM. The p values were determined by Student's t test (unpaired two-tailed) or ANOVA multiple comparison test (Sidák's test) when mentioned, n.s. (non-significant), * $p < 0.05$, ** $p < 0.01$ and *** $p < 0.001$, **** $p < 0.0001$.

wildtype (WT) or *KP* mice (not shown).³⁴ The mutant alleles were then crossed to the aforementioned tumor models to generate homozygous *Trp53* null mice (referred to as *KPC^{fl/fl}*). The models were further validated by confirming the specific loss of exon 3a and 3c upon Cre recombination (Figure S3E). *KPC^{fl/fl}* mice developed highly aggressive invasive PDAC with a short life span and median survival of 8 weeks. Genetic deletion of *KhkC*, *KhkA* or *KhkA/C* in this model revealed similar tumor weights at 8 weeks and similar overall survival (Figures S3F and S3G). As previously shown, *KPC* mice driven by *Trp53^{lox/+}* developed advanced invasive PDAC tumors with a median survival of 24 weeks. Surprisingly *KhkC* and *KhkA/C* deletion in a model with *Trp53* haploinsufficiency strongly reduced the tumor proliferation as shown by Ki67 stainings and tumor weight. In addition, these mice had a prolonged median survival of 28 weeks and 30 weeks, respectively, even under normal chow diet conditions (Figures 3D–3G).

We next generated organoids with *KhkC*, *KhkA*, and *KhkA/C* deletions from *KPC* mice. Gene expression analysis from mouse organoids confirmed the loss of respective alleles (Figure 3H). We measured marked decreases in the expression of *Hk1*, *Hk2*, *Ldha*, *Got1* and *Pkm2*, all involved in glucose metabolism, in *KPC;KhkC^{-/-}* and *KPC;KhkA/C^{-/-}* organoids compared to control *KPC* organoids in normal growth condition without high fructose. While these transcripts were not altered in *KPC;KhkA^{-/-}* organoids, they markedly upregulated the expression of *Mdh2* and *Myc* (Figure 3I). In line with the *in vivo* results, *KhkC* depletion was sufficient to impair the growth of *KPC* organoids *in vitro*, leading to a growth phenotype similar to *KP* and *KPC;KhkA/C^{-/-}* organoids. In contrast, no differences were measured in cell viability of *KPC;KhkA^{-/-}* compared to control *KPC* organoids (Figure 3J).

Pancreatic ablation of *KhkC* strongly dampens the proliferation and migration of *KPC* driven tumors in a cell autonomous manner

To determine the role of *KhkC* and its contribution to less aggressive PDAC tumor phenotypes, we sorted Epcam+ epithelial cells from mouse tumors of all four genotypes, followed by 2D-culturing and performing proliferation and cell migration assays. Similar to the 3D *in vitro* organoid models, *KPC;KhkC^{-/-}* and *KPC;KhkA/C^{-/-}* cells exhibited decreased growth rates compared to *KPC;KhkA^{-/-}* and *KPC* cells. In addition, by employing a scratch assay, we noted a significant decrease in the migratory capability of cells derived from *KPC;KhkC^{-/-}* and *KPC;KhkA/C^{-/-}* tumors (Figures 4A and 4B). These results were corroborated *in vivo* by employing PDAC xenograft models of all four genotypes, which showed a significant reduction in tumor volume and tumor weight from *KPC;KhkC^{-/-}* and *KPC;KhkA/C^{-/-}* compared to *KPC* or *KPC;KhkA^{-/-}* mice (Figures 4C and 4D). These results confirm that the specific inactivation of the *KhkC* isoform is sufficient to reduce the growth of PDAC xenograft tumors in a cell autonomous manner, even in absence of a high fructose diet.

KPC and *KPC;KhkA^{-/-}* organoids treated with a high-fructose diet showed enhanced cell viability compared to the organoids treated only with high glucose (Figure 4E). In high glucose conditions, quantitative RT-PCR analysis revealed reduced expression of *AldoB* in *KPC;KhkC^{-/-}* and *KPC;KhkA/C^{-/-}* organoids, but not in *KPC;KhkA^{-/-}* cells compared to *KPC*. In high-fructose conditions, *AldoB* levels were only significantly repressed in *KPC;KhkC^{-/-}* compared to *KPC* cells (Figures 4F and G), while *AldoB* levels were even higher expressed in *KPC;KhkA^{-/-}* compared to *KPC* organoids. This suggests that in the absence of *KhkC*, induction of *AldoB* is diminished due to decreased fructose metabolism, and conversely, lack of *KhkA* leads to increased *AldoB* expression, likely due to enhanced fructose metabolism. Interestingly, expression of genes involved in acetate metabolism and fatty acid synthesis, *Acsc1* and *Acacb*, were reduced upon deletion of *KhkC* or *KhkA/C*. Transcript levels of genes involved in cholesterol metabolism, including *Srebf2* and *Sqle* were decreased only in *KPC;KhkC^{-/-}* and *KPC;KhkA/C^{-/-}*, while transcripts of *de*

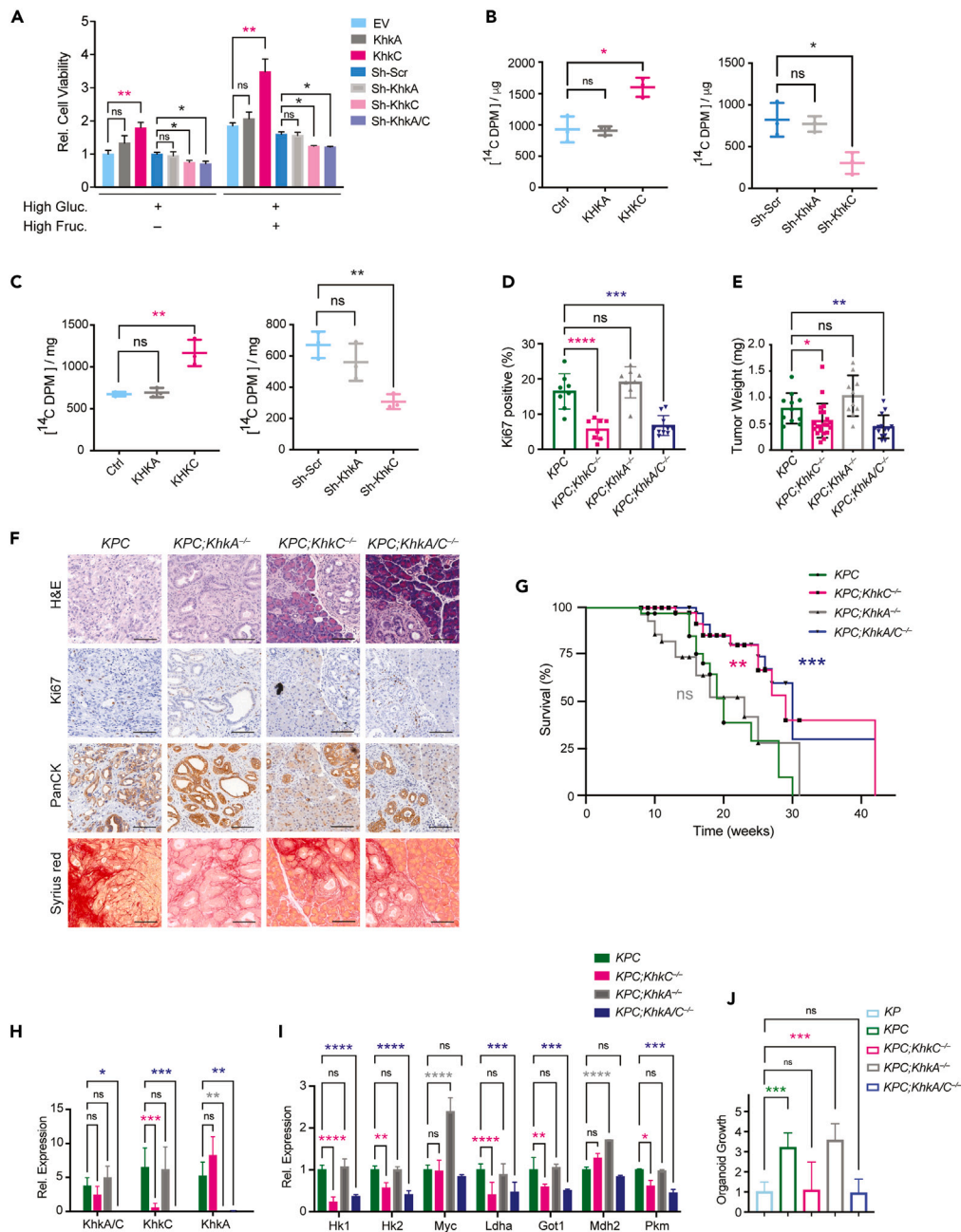


Figure 3. KHKC overexpression promotes tumor growth and *KhkC* KO is sufficient to delay the onset and development of tumors

(A) *KhkA* or *KhkC* was either over-expressed or downregulated by shRNAs in KPC organoids and cell viability was measured after a 48-h incubation in media with or without fructose, n = 3. ANOVA multiple comparison test (Tukey's test). (B) [¹⁴C] fructose incorporation into DNA in KPC organoids overexpressing empty vector (Ctl), *KhkA* or *KhkC*, or after knockdown using sh-Scr (Scramble control) sh-*KhkA* or sh-*KhkC*, respectively after a 16 h incubation, n = 3. (C) [¹⁴C] fructose incorporation measurements into protein of KPC organoids overexpressing empty vector (Ctl), *KhkA* or *KhkC* or after knockdown using sh-Scr (Scramble control) sh-*KhkA* or sh-*KhkC*, respectively, following a 16 h incubation, n = 3. (D) Percentage of Ki67 positivity in mouse tumor sections with the indicated genotype, n = 34 in total. ANOVA multiple comparison test (Tukey's test). (E) Evaluation of pancreas tumor weight from mice with the indicated genotypes at 20 weeks of age, n = 57. ANOVA multiple comparison test (Tukey's test).

Figure 3. Continued

- (F) Representative IHC images of H&E, Ki67, PanCK and Sirius red staining from *KPC*, *KPC;KhkC^{-/-}*; *KPC;KhkA^{-/-}*; *KPC;KhkA/C^{-/-}* tumors at 20 weeks of age.
- (G) Percentage of survival of *KPC*, *KPC;KhkC^{-/-}*; *KPC;KhkA^{-/-}*; *KPC;KhkA/C^{-/-}* mice, n = 149. Kaplan-Meier survival curves were compared by Mantel-Cox log rank test.
- (H) Relative transcript levels of *KhkA/C*, *KhkC*, *KhkA* from mouse organoids derived from the indicated genotypes.
- (I) Relative transcript levels of metabolism genes from organoids of all four aforementioned genotypes.
- (J) Growth measurements of organoids from all indicated genotypes cultured for 4 days in 17.3 mM glucose, n = 6. ANOVA multiple comparisons test (Tukey's test). Data are represented as Mean ± SEM. The p values were determined by Student's t test (unpaired two-tailed) or ANOVA multiple comparison test (Tukey's test) when mentioned, n.s. (non-significant), *p < 0.05, **p < 0.01 and ***p < 0.001, ****p < 0.0001.

novo lipogenesis showed similar expression levels, with the exception of the fatty acid oxidation gene *Cpt1α*, which was decreased upon inactivation of *KhkA/C* (Figure 4H). When challenging the mutant mice of the four aforementioned genotypes with a high fructose diet for 10 weeks and comparing them to chow diets, we measured increased proliferation and tumor weight only in *KPC* mouse tumors. Inhibition of proliferation was greater in all KHK-mutant genotypes under high fructose conditions, and even *KPC;KhkA^{-/-}* tumors showed no significant increase in Ki67 stainings compared to *KPC* control mice fed a high fructose diet, suggesting that under fructose stress both isoforms are required for tumor growth (Figures S4A–S4C). These effects could not be ascribed to changes in blood insulin and glucose, as there was no significant difference at 20 weeks of age (Figures S4D and S4E). Lastly, genetic inactivation of *KhkC* and *KhkA/C* profoundly reduced the overall survival of *KPC* mice even upon fructose diet, while *KhkA* ablation showed no significant difference (Figure S4F). These results demonstrate that dietary fructose enhances the proliferation of *KPC*-driven tumors *in vitro* and *in vivo* in a cell autonomous manner and that *KhkC* deletion is sufficient to reduce the growth and the migration of pancreatic cancer cells, leading to lower expression of fructose metabolizing genes downstream of KHK.

Pancreatic *KhkC* inactivation rewires PDAC metabolism-related pathways

To investigate the mechanisms by which KHK and its isoforms influence PDAC development, we performed RNA seq from sorted Epcam+; CD45- cancer cells of age-matched *KPC* mouse tumors and from tumors with genetic ablation of *KhkC*, *KhkA* and *KhkA/C* (Figures 5A and S5A). Hallmark gene set analyses from all four genotypes showed a significant reduction of cell cycle, inflammation, damage response, metabolism and cell signaling pathways, including *Kras* and mTORC1 signaling pathways, in tumors of both *KPC;KhkC^{-/-}* and *KPC;KhkA/C^{-/-}* mice compared to *KPC* and *KPC;KhkA^{-/-}* tumor cells (Figure S5B). Surprisingly, in the absence of a high fructose diet we measured higher expression levels of genes involved in pathways related to inflammation, damage response, cell cycle, metabolism, and mTORC1, *Kras* and Tgfβ signaling in *KPC;KhkA^{-/-}* compared to *KPC* alone, *KPC;KhkC^{-/-}* or *KPC;KhkA/C^{-/-}* tumor cells. Similarly, KEGG pathway analysis of *KPC;KhkA^{-/-}* versus *KPC;KhkC^{-/-}* confirmed a significant upregulation of pathways involved in cell cycle, DNA replication, pathways linked to fructose, mannose and galactose metabolism, pentose phosphate pathway, purine and pyrimidine metabolism, as well as nicotinate and nicotinamide metabolism, supporting a fundamental role for the *KhkC* isoform in key pathways involved in PDAC progression (Figures 5B and 5C).

Of note, analysis of organoids derived from *KPC;KhkC* and *KPC;KhkA/C* KO tumors confirmed a strong downregulation of the KRAS/MAPK pathway, as shown by lower expression of activated ERK1/2 (phospho-ERK1/2 Thr202/Tyr204) (Figure 5D). mTOR, a key downstream effector pathway of RAS^{35,36} involved in cell growth and protein synthesis,^{35,36} was strongly reduced in both *KPC;KhkC^{-/-}* and *KPC;KhkA/C^{-/-}* tumors, as shown by reduced expression of phospho-RPS6 in immunoblot analysis and by immunofluorescence staining of mouse tumor cells treated with mTOR inhibitor rapamycin, as well as from mouse tumor tissue sections (Figures 5D, 5E and S5C). Untargeted metabolomics from mouse tumor cell lines treated with low glucose (3 mM) and high fructose (1 mM) for 48 h confirmed numerous changes in metabolites between the *KPC;KhkC^{-/-}* and *KPC;KhkA^{-/-}*. Specifically, analysis of *KPC;KhkC^{-/-}* showed an accumulation of glucose, fructose 6-phosphate, NAD, NADPH, phosphocreatine, ribulose 5-phosphate (an intermediate of the non-oxidative arm of PPP), pyruvic acid and acetyl-CoA, compared to *KPC;KhkA^{-/-}* cells (Figure 5F). In addition, glycine, isoleucine, L-homoserine levels were increased, while different species of lipids were downregulated in *KPC;KhkC^{-/-}* compared to *KPC;KhkA^{-/-}*, indicating an inverse correlation between gene expression and metabolites, most likely due to their different metabolic consumption rate and

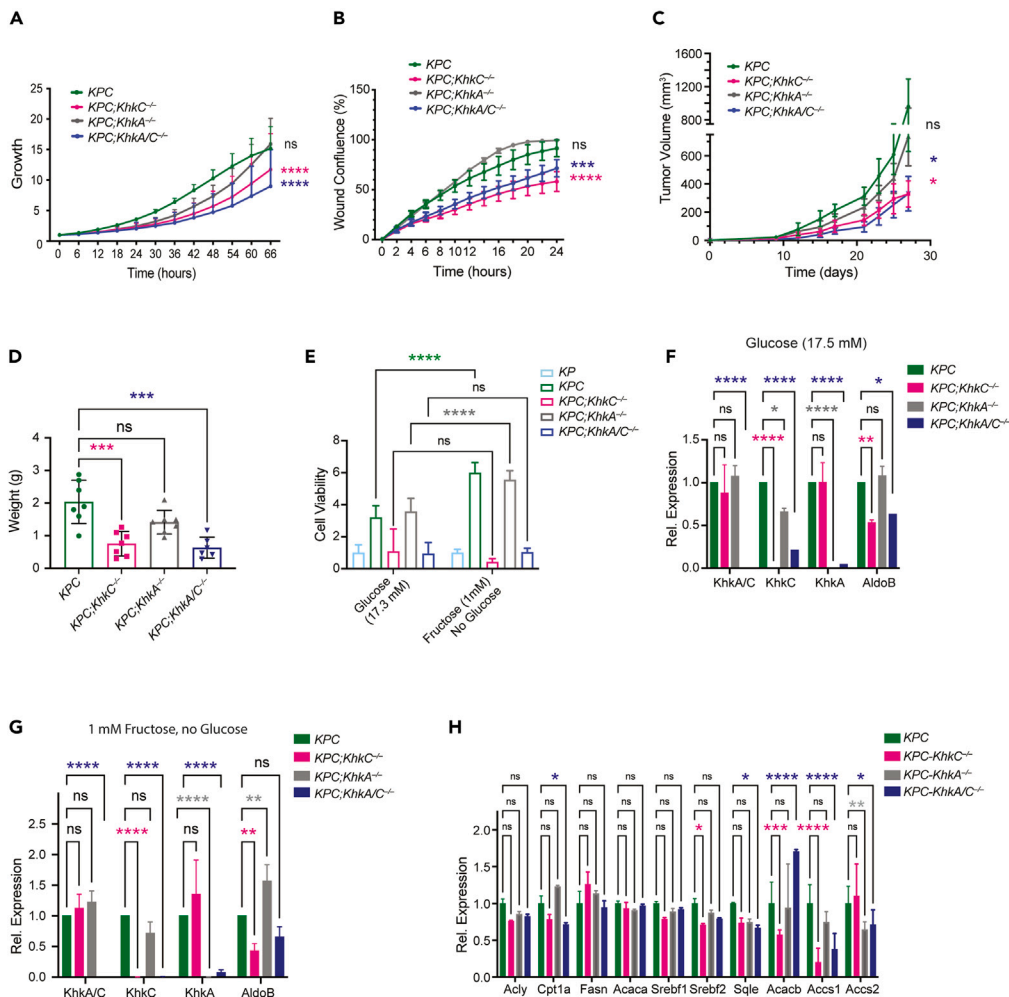


Figure 4. Pancreatic ablation of *KhkC* dampens the proliferation and migration of KPC driven tumors in a cell autonomous manner

(A) Cell proliferation measurements of mouse derived cancer cells of *KPC*, *KPC;KhkC*^{-/-}; *KPC;KhkA*^{-/-}; *KPC;KhkA/C*^{-/-}, determined by live-cell imaging analysis for 66 h, ANOVA multiple comparison test (Tukey's test), n = 3.

(B) Cell migration measurements of mouse derived *KPC*, *KPC;KhkC*^{-/-}; *KPC;KhkA*^{-/-}; *KPC;KhkA/C*^{-/-} cancer cells, determined by live-cell imaging analysis of wound healing confluence for 24 h. ANOVA multiple comparison test (Tukey's test), n = 3.

(C) Fold-change of the tumor volume (mm³) of *KPC*, *KPC;KhkC*^{-/-}; *KPC;KhkA*^{-/-}; *KPC;KhkA/C*^{-/-} cancer cells. ANOVA multiple comparison test (Tukey's test), n = 8.

(D) Tumor weight endpoints (in g) from *KPC*, *KPC;KhkC*^{-/-}; *KPC;KhkA*^{-/-}; *KPC;KhkA/C*^{-/-} xenograft tumors. ANOVA multiple comparison test (Tukey's test), n = 7.

(E) Cell viability measurements from *KPC*, *KPC;KhkC*^{-/-}; *KPC;KhkA*^{-/-}; *KPC;KhkA/C*^{-/-} mouse tumors organoids upon treatment with high glucose (17.3 mM) and high fructose (1 mM) for 4 days.

(F) Relative transcript levels of *KhkA/C*, *KhkC*, *KhkA* and *AldoB* organoids treated with high glucose (17.3 mM).

(G) Relative transcript levels of *KhkA/C*, *KhkC*, *KhkA* and *AldoB* from organoids of the indicated genotypes treated with high fructose (1 mM).

(H) Gene expression analysis of fatty acid oxidation and lipid metabolism in high glucose diet from *KPC*, *KPC;KhkC*^{-/-}, *KPC;KhkA*^{-/-}, and *KPC;KhkA/C*^{-/-} organoids. ANOVA multiple comparison test (Tukey's test), n = 3. Data are represented as Mean ± SEM. The p values were determined by Student's t test (unpaired two-tailed) or ANOVA multiple comparison test (Tukey's test) when mentioned, n.s. (non-significant), *p < 0.05, **p < 0.01 and ***p < 0.001, ****p < 0.0001.

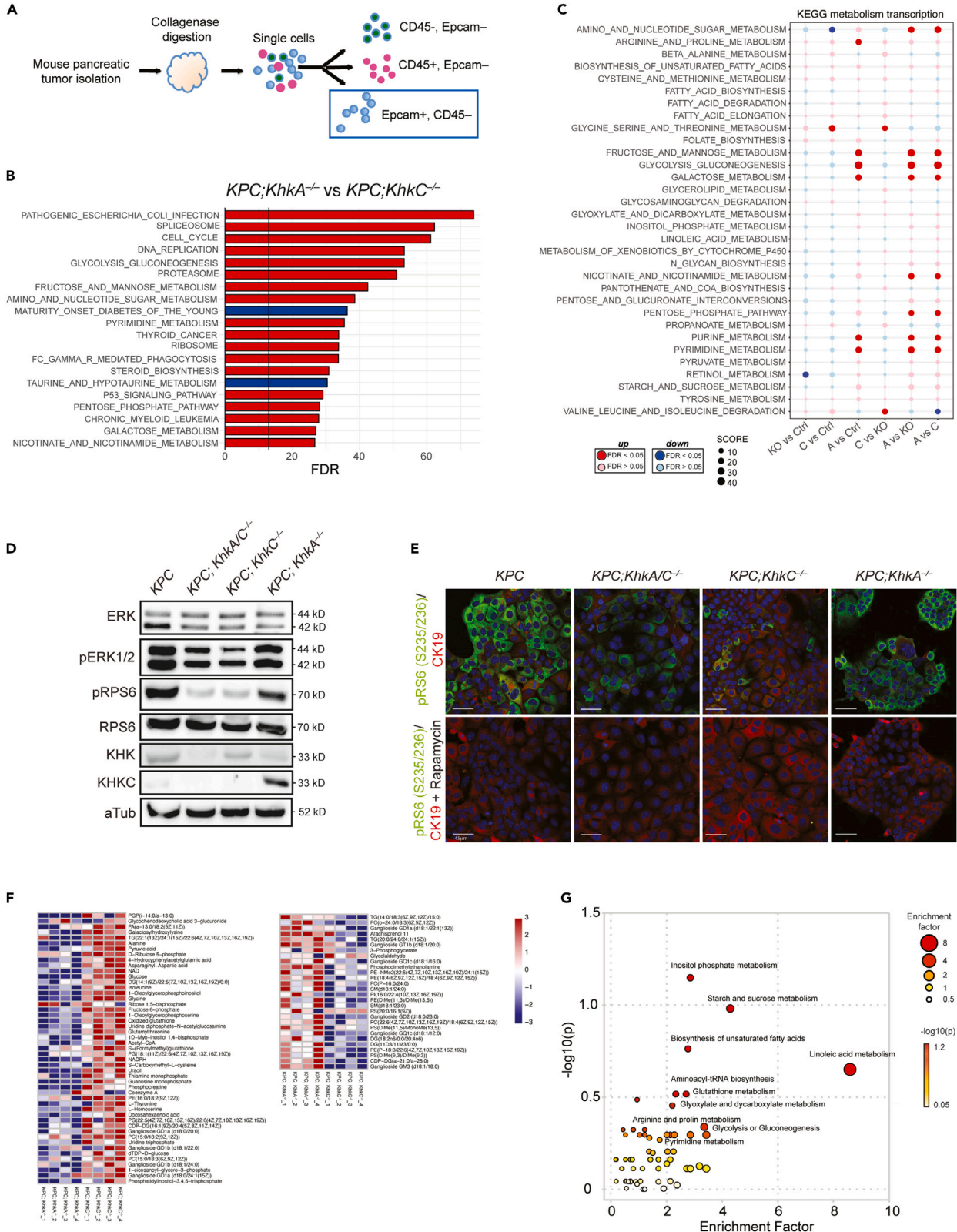


Figure 5. Pancreatic *KhkC* inactivation rewires PDAC metabolism-related pathways

(A) Schematic of sorting strategy of Epcam⁺; CD45⁻ cells from *KPC*, *KPC;KhkC^{-/-}*, *KPC;KhkA^{-/-}*, and *KPC;KhkA/C^{-/-}* mouse tumors at 20 weeks of age. (B) Gene set enrichment analysis (GSEA) on the most regulated KEGG pathways from RNA-seq analysis of Epcam⁺; CD45⁻ *KPC;KhkA^{-/-}* and *KPC;KhkC^{-/-}* mouse tumor cells (n = 2). p values are expressed in form of $-10 \times \log_{10}$ FDR (FDR-adjusted). Upregulated: red; downregulated: blue. (C) Dot plots representing a KEGG analysis of metabolic pathways from *ex vivo* Epcam⁺; CD45⁻ cells transcriptomics analysis. (*KPC*: n = 3; *KPC;KhkA/C^{-/-}*: n = 3; *KPC;KhkC^{-/-}*: n = 2; *KPC;KhkA^{-/-}*: n = 2). p values are expressed in form of $-10 \times \log_{10}$ FDR (FDR-adjusted). Upregulated: red; downregulated: blue. (D) Representative Western blot of *KPC*, *KPC;KhkC^{-/-}*, *KPC;KhkA^{-/-}*, and *KPC;KhkA/C^{-/-}* mouse tumors cells showing the downregulation of p-ERK1/2 and p-RPS6. (E) Representative IF images from *KPC*, *KPC;KhkC^{-/-}*, *KPC;KhkA^{-/-}*, and *KPC;KhkA/C^{-/-}* cancer cells showing CK19 and phospho RpS6 expression (upper panel), and validation by treatment for 16 h with Rapamycin (lower panel). Scale bar: 45 μ m. (F) Heatmap showing the quantification of LC-MS metabolites of *KPC;KhkC^{-/-}* and *KPC;KhkA^{-/-}* cancer cell lines upon high fructose treatment for 48 h, n = 4. (G) Bubble chart of KEGG pathway enrichment. The size and color of each circle indicate the significance of the pathway ranked by p value (red: higher p values and yellow: lower p values) and enrichment factor (the larger the circle the higher the impact score), respectively.

growth. To perform metabolic pathway enrichment analysis, the human metabolome database (HMDB) ID's of annotated metabolites from our input list were fed into the MetaboAnalyst database.^{37–39} A wide range of metabolic pathways were assigned as functionally enriched or over-represented, and between those, 11 were significantly enriched in *KPC;KhkC^{-/-}* and *KPC;KhkA^{-/-}* tumor cells, including inositol phosphate metabolism biosynthesis of unsaturated fatty acids, starch and sucrose metabolism, glyoxylate and dicarboxylate metabolism, glutathione metabolism, aminoacyl-tRNA biosynthesis, linoleic acid metabolism, glycolysis or gluconeogenesis, and pyrimidine metabolism (Figure 5G). Metabolic pathways that were predicted from RNA-seq data and related to metabolomic enrichments in cells from *KPC;KhkA^{-/-}* tumors confirmed an up regulation of interconnected biochemical reactions of glycolysis, gluconeogenesis and pyrimidine metabolism compared to *KPC;KhkC^{-/-}* tumor cells (Figure S5D). These data suggest that *KhkC* KO, and to similar extent *KhkA/C* KO, impairs Kras/MAPK and mTORC pathway gene expression and the activation of ERK1/2 and RPS6, rewires the expression of PDAC-related metabolism and signaling pathways, thereby impairing tumor progression.

DISCUSSION

Radical surgical resection combined with perioperative chemotherapy remains the only potentially curative option for PDAC patients. However, the recurrence rate is high, underscoring the need for better adjuvant therapies to improve long-term survival. Transformed cells rewire their metabolism to support tumor initiation and progression and often rely on critical nutrient sources. Therefore, exploiting the reprogrammed cancer metabolism provides an innovative therapeutic strategy. Epidemiological studies suggest that fructose consumption confers a greater pancreatic cancer risk than other sugars.^{40–42}

KHKC is produced primarily in the liver, intestine, and kidneys, which efficiently metabolizes fructose and fuel gluconeogenesis, glycogen, triglyceride, and purine synthesis.¹⁹ In line with this observation are several human and rodent studies showing a correlation of fructose consumption with tumor growth in these tissues and profound effects on tumor growth when fructose metabolism is impaired.^{24,26,27,42–47} Increased fructose uptake contributes to enhance cellular survival and proliferation in many cancers.^{12,23} However, the function of specific KHK isoforms during cancerogenesis is still poorly understood. In cancers such as liver and breast cancer, both KHK isoforms have been shown to have distinct roles.^{25,26,48} In HCC, fructose metabolism appears to be inhibitory and is reduced in HCC cells through a mechanism involving c-myc-dependent transcriptional activation of hnRNP H1/2, which mediates a switch of the KHKC to the KHKA isoform.¹⁶ Using the *MUP-uPA* mouse model of NASH-driven HCC, a recent report demonstrated that consumption of a high-fructose diet promoted HCC development through a mechanism involving ER-stress-dependent barrier deterioration in the colon, endotoxemia and deterioration of steatohepatitis through activation of TLR signaling in liver macrophages.¹⁷ In breast cancer, overexpression of the KHKA isoform induced metastasis through 14-3-3 phosphorylation and recruitment of SLUG to the Cadherin 1 (*CDH1*) promoter under fructose-fed conditions, suggesting that KHKA, rather than KHKC, is necessary and sufficient for fructose-induced cell invasion.⁴⁸

The impact of fructose metabolism in tumors derived from tissues with low KHKC expression is unknown. We and others have shown that KHK expression in the pancreas is markedly lower compared to liver and kidneys in normal pancreas, blurring its physiological relevance in physiological and malignant conditions. Whether dietary fructose effects are indirect or could also be explained by cell autonomous fructose

metabolizing mechanisms is unknown, as no reports have yet addressed the specific role of KHK and its isoforms in PDAC development or in other cancerous tissues derived from organs with low KHK activity. Here, we show that KHK expression is induced in human PDAC tissue sections and in mouse *KPC* tumors that fully recapitulate pancreatic cancer. Furthermore, we demonstrate that fructose metabolism-related genes are overexpressed together with *Khk* in *KPC* tumor compared to the *KP* mouse organoids. *Khk* and the fructose metabolism-related gene expression are also enhanced upon hypoxia, a key feature of PDAC development.⁴⁹ Moreover we show that high dietary fructose enhances the proliferation and decreases the overall survival due to the increase of KHK activity and higher expression of KHKC. Indeed, overexpression of the *KhkC* isoform in mouse *KPC* cells induces higher cell viability *in vitro* that results in even more viability upon high fructose treatment compared to *KhkA* overexpression. Using newly developed conditional mouse models of *KhkC* or *KhkA* deletion in the pancreas, we demonstrate that *KhkC* inactivation is sufficient to delay the onset and the development of PDAC, and significantly enhances the overall survival of *KPC*-driven tumor models, even in absence of high dietary fructose. These results emphasize an important role of KHK activity in PDAC despite its low expression in the normal pancreas.

Our study also revealed that loss of KHKC function decreases the viability of *KPC* organoids and cancer cells, the migratory capability of PDAC cells *in vitro*, and the growth of *KPC* cells *in vivo* in a cell autonomous manner when injected in immunodeficient mice. It is likely that these effects are mediated at least in part by the impaired activation of KRAS-MAPK pathway upon inactivation of KHKC or all KHK isoforms, as shown by the downregulation of phospho-ERK1/2 and by a decreased activation of RPS6, a downstream target of mTORC pathway. Conversely, we demonstrate that overexpression of KHKC in *KPC* cells enhances KRAS downstream pathway, while KHKC overexpression acts as a tumor suppressor by blocking the phosphorylation of ERK1/2 and decreasing RPS6 activation. In line with these findings, we found that transcriptomics data of Epcam+ CD45- sorted *ex vivo* cancer cells confirmed the regulation of mTORC1 and KRAS pathways as well as EMT and MYC targets genes, which were impaired in *KPC;KhkC^{-/-}* compared to *KPC;KhkA^{-/-}* or *KPC* tumor cells. Interestingly *KPC;KhkA^{-/-}* transcriptomics data revealed an opposite regulation of the transcription of genes compared to *KPC;KhkC^{-/-}* and to *KPC* involved in cell cycle and growth and more importantly in cell metabolism such as fructose and mannose metabolism, glycolysis, galactose metabolism and purine and pyrimidine metabolism, which could be accounted for enhanced fructose metabolism through KHKC overexpression. Metabolomics data analysis on cancer cells derived from our mouse models and treated with high fructose highlight an accumulation of many metabolites involved in glycolysis, pentose phosphate pathway in *KPC;KhkC^{-/-}* compared to *KPC;KhkA^{-/-}*, suggesting altered consumption rates of these cells linked to their growth. Recent reports suggest that knocking down fructose metabolism by deleting KHK suppresses cancer growth in response to HFCS in APC mice.²⁴ Furthermore, PF-06835919, a KHK inhibitor was developed and tested in a phase 2 clinical trial for NAFLD.⁵⁰ The compound resulted in pronounced fructosuria, and reduced intrahepatic lipid in adults with NAFLD.⁵¹ Other reports have also shown that a ketogenic diet (low carbohydrates, low protein, high fat) results in increased intracellular NADH, priming PDAC cells for treatment with chemotherapy and leading to cytotoxicity and tumor regression.⁵² Here, we unraveled a potential role of KHK in early PDAC development and progression and propose KHK as a therapeutic target for adjuvant treatment of PDAC progression.

In summary, our findings show that increased KHKC expression in PDAC promotes its development and progression and that genetic inactivation of the KHKC isoform impairs fundamental pathways for PDAC growth and progression by impacting on key signaling and metabolic pathways, including KRAS-MAPK and mTORC signaling as well as glycolysis, pentose phosphate pathway, and pyrimidine/purine metabolism. Given the fact that existing inhibitors targeting KHK have been tested in clinical trials for nonalcoholic steatohepatitis (NASH), it would be of interest to analyze their effects as adjuvant therapies on PDAC patients. Together, our findings suggest that therapeutic targeting of KHK and fructose metabolism may be a strategy for slowing the progression of PDAC even in the absence of high dietary fructose intake.

Limitations of the study

We point out that we have not been able to show increased expression of KHKC protein in biopsies of human pancreatic tumors because we did not have access to suitable antibody for immunohistochemical stainings. Furthermore, it would be important to investigate the role of KHKC and KHKC isoforms in cancer cell lines derived from pancreatic cancers. In addition, organoids from human PDAC with defined driver genes, in combination with CRISPR-based approaches to obtain genetic knock-outs of KHK-specific

isoforms, will be a powerful system to study the role of KHK in human PDAC and validate our findings in the mouse.

STAR★METHODS

Detailed methods are provided in the online version of this paper and include the following:

- KEY RESOURCES TABLE
- RESOURCE AVAILABILITY
 - Lead contact
 - Materials availability
 - Data and code availability
- EXPERIMENTAL MODEL AND SUBJECT DETAILS
 - Mouse models
 - Human sample collection
 - Pancreatic cancer cell culture
 - Human PDAC organoid culture
 - Murine PDAC organoid culture
- METHOD DETAILS
 - Organoid proliferation assays
 - 2D cell proliferation assay
 - Migration assay
 - Plasmid constructions of over-expression and shRNAs knockdown of KhkA, KhkC and KhkA/C
 - Lentivirus production and transduction
 - Insulin Elisa assay
 - Glucose measurement
 - Immunohistochemistry (IHC) and immunofluorescence (IF)
 - Ketohexokinase activity assay
 - [¹⁴C (U)] D-fructose incorporation into DNA and protein *in vitro*
 - Western blot
 - Antibodies
 - EdU incorporation assays
 - Real-time PCR analysis
 - Fructose or glucose feeding
 - Analysis of metabolites in cancer cell lines
 - Sample preparation for LC-MS analysis and LC-MS analysis
 - Untargeted metabolomics data analysis
 - Illumina RNA sequencing
 - RNA seq data analysis
- QUANTIFICATION AND STATISTICAL ANALYSIS

SUPPLEMENTAL INFORMATION

Supplemental information can be found online at <https://doi.org/10.1016/j.isci.2023.107368>.

ACKNOWLEDGMENTS

This work is dedicated to Willy Krek, our mentor, colleague, and friend, who initiated and supervised the study until he passed away on August 29, 2018. We are grateful to T. Jacks (Koch Institute, MIT, Cambridge/MA, USA) and R. Johnson (University of Colorado) for providing mouse strains and A. Asipu (Leeds, GB) for providing plasmid constructs. We wish to thank Regina Kubsch for excellent technical assistance and all the members of Stoffel lab and former Krek lab. We acknowledge the Functional Genomics Center Zurich for RNA-seq (L. Opitz and S. Kreuzer) and for metabolomics (M. Zanella), the Scientific Center for Optical and Electron Microscopy (ScopeM), the Eidgenössische Technische Hochschule (ETH) Flow Cytometry Core Facility (E-FCCF) for support. We acknowledge support from the Biobank of the European Pancreas Centre at the Department of General and Visceral Surgery of the University Hospital (EPZ-Pancobank), working in accordance with the regulations of the tissue banks and upon an approval of the Ethics Committee of Heidelberg University (Ethic votes S-708/2019 and S-083/2021). Collection & processing of the samples and clinical data by the EPZ- Pancobank was supported by the Heidelberger Stiftung Chirurgie and in part by the German Ministry of Science and Education (BMBF) grants 01ZX1305C,

01ZX1605C, 01KT1506. The EPZ-Pancobank is chaired by Prof. M.W. Büchler assisted by Dr. N.A. Giese, Dr. M. Schenk, M. Fischer, and U. Hinz, and is a member of the BioMaterial Bank Heidelberg (supervisor: Prof. P. Schirmacher, BMBF grant# 01EY1101 and G-BA/BBMRI.de grant 01EY1707) belonging to the German Biobank Alliance. This work was financed by SNSF grant (Grant number: 176317) and the W. Fischli Foundation. IG was in part supported by the SAKK foundation.

AUTHOR CONTRIBUTIONS

Leading: W.K., M.S., and I.G.; Supervision: M.S. and I.G.; Writing – Original Draft: I.G. and M.S.; Writing – Review and Editing: I.G., M.S., A.A., and G.S.; *In vivo* experiments: I.G., G.T., M.D., and E.P.; Investigation: *In vitro* experiments: I.G., G.T., T.T.T., M.D., H.K., and S.G.; Confocal imaging acquisition: P.S.; Bioinformatics: L.D. and M.B.; Clinical samples: S.B. and O.S.; Resources: I.G. and M.S.; Project administration: M.S. All authors read and approved the manuscript.

DECLARATION OF INTERESTS

M.S. is a member of the Scientific Advisory Board of Alnylam Pharmaceuticals. All other authors declare no conflict of interest relating to this study.

INCLUSION AND DIVERSITY

We support inclusive, diverse, and equitable conduct of research.

Received: April 5, 2023

Revised: June 9, 2023

Accepted: July 10, 2023

Published: July 13, 2023

REFERENCES

- Hosein, A.N., Dougan, S.K., Aguirre, A.J., and Maitra, A. (2022). Translational advances in pancreatic ductal adenocarcinoma therapy. *Nat. Cancer* 3, 272–286. <https://doi.org/10.1038/s43018-022-00349-2>.
- Ushio, J., Kanno, A., Ikeda, E., Ando, K., Nagai, H., Miwata, T., Kawasaki, Y., Tada, Y., Yokoyama, K., Numao, N., et al. (2021). Pancreatic ductal adenocarcinoma: epidemiology and risk factors. *Diagnostics* 11, 562. <https://doi.org/10.3390/diagnostics11030562>.
- Hu, H.F., Ye, Z., Qin, Y., Xu, X.W., Yu, X.J., Zhuo, Q.F., and Ji, S.R. (2021). Mutations in key driver genes of pancreatic cancer: molecularly targeted therapies and other clinical implications. *Acta Pharmacol. Sin.* 42, 1725–1741. <https://doi.org/10.1038/s41401-020-00584-2>.
- Biancur, D.E., and Kimmelman, A.C. (2018). The plasticity of pancreatic cancer metabolism in tumor progression and therapeutic resistance. *Biochim. Biophys. Acta. Rev. Cancer* 1870, 67–75. <https://doi.org/10.1016/j.bbcan.2018.04.011>.
- Vander Heiden, M.G., Cantley, L.C., and Thompson, C.B. (2009). Understanding the Warburg effect: the metabolic requirements of cell proliferation. *Science* 324, 1029–1033. <https://doi.org/10.1126/science.1160809>.
- Li, J.T., Wang, Y.P., Yin, M., and Lei, Q.Y. (2019). Metabolism remodeling in pancreatic ductal adenocarcinoma. *Cell Stress* 3, 361–368. <https://doi.org/10.15698/cst2019.12.205>.
- Rippe, J.M., and Angelopoulos, T.J. (2016). Relationship between added sugars consumption and chronic disease risk factors: current understanding. *Nutrients* 8, 697. <https://doi.org/10.3390/nu8110697>.
- Rippe, J.M., and Tappy, L. (2016). Sweeteners and health: findings from recent research and their impact on obesity and related metabolic conditions. *Int. J. Obes.* 40, S1–S5. <https://doi.org/10.1038/ijo.2016.7>.
- Clemente-Suárez, V.J., Mielgo-Ayuso, J., Martín-Rodríguez, A., Ramos-Campo, D.J., Redondo-Flórez, L., and Tornero-Aguilera, J.F. (2022). The burden of carbohydrates in health and disease. *Nutrients* 14, 3809. <https://doi.org/10.3390/nu14183809>.
- Johnson, R.J., Segal, M.S., Sautin, Y., Nakagawa, T., Feig, D.I., Kang, D.H., Gersch, M.S., Benner, S., and Sánchez-Lozada, L.G. (2007). Potential role of sugar (fructose) in the epidemic of hypertension, obesity and the metabolic syndrome, diabetes, kidney disease, and cardiovascular disease. *Am. J. Clin. Nutr.* 86, 899–906. <https://doi.org/10.1093/ajcn/86.4.899>.
- Lim, J.S., Mietus-Snyder, M., Valente, A., Schwarz, J.M., and Lustig, R.H. (2010). The role of fructose in the pathogenesis of NAFLD and the metabolic syndrome. *Nat. Rev. Gastroenterol. Hepatol.* 7, 251–264. <https://doi.org/10.1038/nrgastro.2010.41>.
- Jiang, H., Lin, Q., Ma, L., Luo, S., Jiang, X., Fang, J., and Lu, Z. (2021). Fructose and fructose kinase in cancer and other pathologies. *J. Genet. Genomics* 48, 531–539. <https://doi.org/10.1016/j.jgg.2021.06.006>.
- Jung, S., Bae, H., Song, W.S., Jang, C., Sundaram, S., Jung, S., Bae, H., Song, W.S., and Jang, C. (2022). Dietary fructose and fructose-induced pathologies. *Annu. Rev. Nutr.* 42, 45–66. <https://doi.org/10.1146/annurev-nutr-062220-025831>.
- Jang, C., Hui, S., Lu, W., Cowan, A.J., Morscher, R.J., Lee, G., Liu, W., Tesz, G.J., Birnbaum, M.J., and Rabinowitz, J.D. (2018). The small intestine converts dietary fructose into glucose and organic acids. *Cell Metab.* 27, 351–361.e3. <https://doi.org/10.1016/j.cmet.2017.12.016>.
- Kawabata, K., Kanmura, S., Morinaga, Y., Tanaka, A., Makino, T., Fujita, T., Arima, S., Sasaki, F., Nasu, Y., Tanoue, S., et al. (2019). A high-fructose diet induces epithelial barrier dysfunction and exacerbates the severity of dextran sulfate sodium-induced colitis. *Int. J. Mol. Med.* 43, 1487–1496. <https://doi.org/10.3892/ijmm.2018.4040>.
- Li, X., Qian, X., Peng, L.X., Jiang, Y., Hawke, D.H., Zheng, Y., Xia, Y., Lee, J.H., Cote, G., Wang, H., et al. (2016). A splicing switch from ketohexokinase-C to ketohexokinase-A drives hepatocellular carcinoma formation. *Nat. Cell Biol.* 18, 561–571. <https://doi.org/10.1038/ncb3338>.
- Todoric, J., Di Caro, G., Reibe, S., Henstridge, D.C., Green, C.R., Vrbanac, A., Ceteci, F., Conche, C., McNulty, R., Shalapur, S., et al. (2020). Fructose stimulated *de novo* lipogenesis is promoted by inflammation.

- Nat. Metab. 2, 1034–1045. <https://doi.org/10.1038/s42255-020-0261-2>.
18. Lysiotis, C.A., and Cantley, L.C. (2013). Metabolic syndrome: F stands for fructose and fat. *Nature* 502, 181–182. <https://doi.org/10.1038/502181a>.
 19. Ishimoto, T., Lanaspá, M.A., Le, M.T., García, G.E., Diggle, C.P., Maclean, P.S., Jackman, M.R., Asipu, A., Boncal-Jimenez, C.A., Kosugi, T., et al. (2012). Opposing effects of fructokinase C and A isoforms on fructose-induced metabolic syndrome in mice. *Proc. Natl. Acad. Sci. USA* 109, 4320–4325. <https://doi.org/10.1073/pnas.1119908109>.
 20. Diggle, C.P., Shires, M., Leitch, D., Brooke, D., Carr, I.M., Markham, A.F., Hayward, B.E., Asipu, A., and Bonthron, D.T. (2009). Ketohexokinase: expression and localization of the principal fructose-metabolizing enzyme. *J. Histochem. Cytochem.* 57, 763–774. <https://doi.org/10.1369/jhc.2009.953190>.
 21. Hayward, B.E., and Bonthron, D.T. (1998). Structure and alternative splicing of the ketohexokinase gene. *Eur. J. Biochem.* 257, 85–91. <https://doi.org/10.1046/j.1432-1327.1998.2570085.x>.
 22. Nikolaou, K.C., Vatasdaslar, H., Meyer, C., Schmid, M.W., Tuschl, T., and Stoffel, M. (2019). The RNA-binding protein A1CF regulates hepatic fructose and glycerol metabolism via alternative RNA splicing. *Cell Rep.* 29, 283–300.e8. <https://doi.org/10.1016/j.celrep.2019.08.100>.
 23. Jung, S., Bae, H., Song, W.S., and Jang, C. (2022). Dietary fructose and fructose-induced pathologies. *Annu. Rev. Nutr.* 42, 45–66. <https://doi.org/10.1146/annurev-nutr-062220-025831>.
 24. Goncalves, M.D., Lu, C., Tutnauer, J., Hartman, T.E., Hwang, S.K., Murphy, C.J., Pauli, C., Morris, R., Taylor, S., Bosch, K., et al. (2019). High-fructose corn syrup enhances intestinal tumor growth in mice. *Science* 363, 1345–1349. <https://doi.org/10.1126/science.aat8515>.
 25. Carreño, D.V., Corro, N.B., Cerda-Infante, J.F., Echeverría, C.E., Asencio-Barría, C.A., Torres-Estay, V.A., Mayorga-Weber, G.A., Rojas, P.A., Véliz, L.P., Cisternas, P.A., et al. (2021). Dietary fructose promotes prostate cancer growth. *Cancer Res.* 81, 2824–2832. <https://doi.org/10.1158/0008-5472.CAN-19-0456>.
 26. Chen, W.L., Wang, Y.Y., Zhao, A., Xia, L., Xie, G., Su, M., Zhao, L., Liu, J., Qu, C., Wei, R., et al. (2016). Enhanced fructose utilization mediated by SLC2A5 is a unique metabolic feature of acute myeloid leukemia with therapeutic potential. *Cancer Cell* 30, 779–791. <https://doi.org/10.1016/j.ccell.2016.09.006>.
 27. Jiang, Y., Pan, Y., Rhea, P.R., Tan, L., Gagea, M., Cohen, L., Fischer, S.M., and Yang, P. (2016). A sucrose-enriched diet promotes tumorigenesis in mammary gland in part through the 12-lipoxygenase pathway. *Cancer Res.* 76, 24–29. <https://doi.org/10.1158/0008-5472.CAN-14-3432>.
 28. Bardeesy, N., Aguirre, A.J., Chu, G.C., Cheng, K.H., Lopez, L.V., Hezel, A.F., Feng, B., Brennan, C., Weissleder, R., Mahmood, U., et al. (2006). Both p16(Ink4a) and the p19(Arf)-p53 pathway constrain progression of pancreatic adenocarcinoma in the mouse. *Proc. Natl. Acad. Sci. USA* 103, 5947–5952. <https://doi.org/10.1073/pnas.0601273103>.
 29. Hingorani, S.R., Petricoin, E.F., Maitra, A., Rajapakse, V., King, C., Jacobetz, M.A., Ross, S., Conrads, T.P., Veenstra, T.D., Hitt, B.A., et al. (2003). Preinvasive and invasive ductal pancreatic cancer and its early detection in the mouse. *Cancer Cell* 4, 437–450. [https://doi.org/10.1016/s1535-6108\(03\)00309-x](https://doi.org/10.1016/s1535-6108(03)00309-x).
 30. Hingorani, S.R., Wang, L., Multani, A.S., Combs, C., Deramaudt, T.B., Hruban, R.H., Rustgi, A.K., Chang, S., and Tuveson, D.A. (2005). Trp53R172H and KrasG12D cooperate to promote chromosomal instability and widely metastatic pancreatic ductal adenocarcinoma in mice. *Cancer Cell* 7, 469–483. <https://doi.org/10.1016/j.ccr.2005.04.023>.
 31. Prasad, N.B., Biankin, A.V., Fukushima, N., Maitra, A., Dhara, S., Elkhoulou, A.G., Hruban, R.H., Goggins, M., Leach, S.D., Prasad, N.B., et al. (2005). Gene expression profiles in pancreatic intraepithelial neoplasia reflect the effects of Hedgehog signaling on pancreatic ductal epithelial cells. *Cancer Res.* 65, 1619–1626. <https://doi.org/10.1158/0008-5472.CAN-04-1413>.
 32. Yang, X., Xu, L., Yang, Y.E., Xiong, C., Yu, J., Wang, Y., and Lin, Y. (2020). Knockdown of ribosomal protein S6 suppresses proliferation, migration, and invasion in epithelial ovarian cancer. *J. Ovarian Res.* 13, 100. <https://doi.org/10.1186/s13048-020-00707-7>.
 33. Yi, Y.W., You, K.S., Park, J.S., Lee, S.G., and Seong, Y.S. (2021). Ribosomal protein S6: a potential therapeutic target against cancer? *Int. J. Mol. Sci.* 23, 48. <https://doi.org/10.3390/ijms23010048>.
 34. Diggle, C.P., Shires, M., McRae, C., Crellin, D., Fisher, J., Carr, I.M., Markham, A.F., Hayward, B.E., Asipu, A., and Bonthron, D.T. (2010). Both isoforms of ketohexokinase are dispensable for normal growth and development. *Physiol. Genom.* 42A, 235–243. <https://doi.org/10.1152/physiolgenomics.00128.2010>.
 35. Yang, X., Yang, C., Farberman, A., Rideout, T.C., de Lange, C.F.M., France, J., and Fan, M.Z. (2008). The mammalian target of rapamycin-signaling pathway in regulating metabolism and growth. *J. Anim. Sci.* 86, E36–E50. <https://doi.org/10.2527/jas.2007-0567>.
 36. Saxton, R.A., and Sabatini, D.M. (2017). mTOR signaling in growth, metabolism, and disease. *Cell* 168, 960–976. <https://doi.org/10.1016/j.cell.2017.02.004>.
 37. Chong, J., Wishart, D.S., and Xia, J. (2019). Using metaboanalyst 4.0 for comprehensive and integrative metabolomics data analysis. *Curr. Protoc. Bioinformatics* 68, e86. <https://doi.org/10.1002/cpbi.86>.
 38. Pang, Z., Chong, J., Zhou, G., de Lima Morais, D.A., Chang, L., Barrette, M., Gauthier, C., Jacques, P.E., Li, S., and Xia, J. (2021). MetaboAnalyst 5.0: narrowing the gap between raw spectra and functional insights. *Nucleic Acids Res.* 49, W388–W396. <https://doi.org/10.1093/nar/gkab382>.
 39. Pang, Z., Zhou, G., Ewald, J., Chang, L., Hacariz, O., Basu, N., and Xia, J. (2022). Using MetaboAnalyst 5.0 for LC-HRMS spectra processing, multi-omics integration and covariate adjustment of global metabolomics data. *Nat. Protoc.* 17, 1735–1761. <https://doi.org/10.1038/s41596-022-00710-w>.
 40. Hui, H., Huang, D., McArthur, D., Nissen, N., Boros, L.G., and Heaney, A.P. (2009). Direct spectrophotometric determination of serum fructose in pancreatic cancer patients. *Pancreas* 38, 706–712. <https://doi.org/10.1097/MPA.0b013e3181a7c6e5>.
 41. Larsson, S.C., Bergkvist, L., and Wolk, A. (2006). Consumption of sugar and sugar-sweetened foods and the risk of pancreatic cancer in a prospective study. *Am. J. Clin. Nutr.* 84, 1171–1176. <https://doi.org/10.1093/ajcn/84.5.1171>.
 42. Michaud, D.S., Liu, S., Giovannucci, E., Willett, W.C., Colditz, G.A., and Fuchs, C.S. (2002). Dietary sugar, glycemic load, and pancreatic cancer risk in a prospective study. *J. Natl. Cancer Inst.* 94, 1293–1300. <https://doi.org/10.1093/jnci/94.17.1293>.
 43. Gao, W., Li, N., Li, Z., Xu, J., and Su, C. (2018). Ketohexokinase is involved in fructose utilization and promotes tumor progression in glioma. *Biochem. Biophys. Res. Commun.* 503, 1298–1306. <https://doi.org/10.1016/j.bbrc.2018.07.040>.
 44. Monzavi-Karbassi, B., Hine, R.J., Stanley, J.S., Ramani, V.P., Carcel-Trullols, J., Whitehead, T.L., Kelly, T., Siegel, E.R., Artaud, C., Shaaf, S., et al. (2010). Fructose as a carbon source induces an aggressive phenotype in MDA-MB-468 breast tumor cells. *Int. J. Oncol.* 37, 615–622. <https://doi.org/10.3892/ijo.00000710>.
 45. Su, C., Li, H., and Gao, W. (2018). GLUT5 increases fructose utilization and promotes tumor progression in glioma. *Biochem. Biophys. Res. Commun.* 500, 462–469. <https://doi.org/10.1016/j.bbrc.2018.04.103>.
 46. Terry, P.D., Jain, M., Miller, A.B., Howe, G.R., and Rohan, T.E. (2003). Glycemic load, carbohydrate intake, and risk of colorectal cancer in women: a prospective cohort study. *J. Natl. Cancer Inst.* 95, 914–916. <https://doi.org/10.1093/jnci/95.12.914>.
 47. Weng, Y., Zhu, J., Chen, Z., Fu, J., and Zhang, F. (2018). Fructose fuels lung adenocarcinoma through GLUT5. *Cell Death Dis.* 9, 557. <https://doi.org/10.1038/s41419-018-0630-x>.
 48. Kim, J., Kang, J., Kang, Y.L., Woo, J., Kim, Y., Huh, J., and Park, J.W. (2020). Ketohexokinase-A acts as a nuclear protein kinase that mediates fructose-induced metastasis in breast cancer. *Nat. Commun.* 11, 5436. <https://doi.org/10.1038/s41467-020-19263-1>.

49. Yamasaki, A., Yanai, K., and Onishi, H. (2020). Hypoxia and pancreatic ductal adenocarcinoma. *Cancer Lett.* 484, 9–15. <https://doi.org/10.1016/j.canlet.2020.04.018>.
50. Futatsugi, K., Smith, A.C., Tu, M., Raymer, B., Ahn, K., Coffey, S.B., Dowling, M.S., Fernando, D.P., Gutierrez, J.A., Huard, K., et al. (2020). Discovery of PF-06835919: a potent Inhibitor of Ketohexokinase (KHK) for the treatment of metabolic disorders driven by the overconsumption of fructose. *J. Med. Chem.* 63, 13546–13560. <https://doi.org/10.1021/acs.jmedchem.0c00944>.
51. Kazierad, D.J., Chidsey, K., Somayaji, V.R., Bergman, A.J., Birnbaum, M.J., and Calle, R.A. (2021). Inhibition of ketohexokinase in adults with NAFLD reduces liver fat and inflammatory markers: a randomized phase 2 trial. *Med (N Y)* 2, 800–813.e3. <https://doi.org/10.1016/j.medj.2021.04.007>.
52. Yang, L., TeSlaa, T., Ng, S., Nofal, M., Wang, L., Lan, T., Zeng, X., Cowan, A., McBride, M., Lu, W., et al. (2022). Ketogenic diet and chemotherapy combine to disrupt pancreatic cancer metabolism and growth. *Med (NY)* 3, 119–136. <https://doi.org/10.1016/j.medj.2021.12.008>.
53. Hirt, C.K., Booij, T.H., Grob, L., Simmler, P., Toussaint, N.C., Keller, D., Taube, D., Ludwig, V., Goryachkin, A., Pauli, C., et al. (2022). Drug screening and genome editing in human pancreatic cancer organoids identifies drug-gene interactions and candidates for off-label treatment. *Cell Genom.* 2, 100095. <https://doi.org/10.1016/j.xgen.2022.100095>.
54. Huch, M., Bonfanti, P., Boj, S.F., Sato, T., Loomans, C.J.M., van de Wetering, M., Sojoodi, M., Li, V.S.W., Schuijers, J., Gracanin, A., et al. (2013). Unlimited *in vitro* expansion of adult bi-potent pancreas progenitors through the Lgr5/R-spondin axis. *EMBO J.* 32, 2708–2721. <https://doi.org/10.1038/emboj.2013.204>.
55. Livak, K.J., and Schmittgen, T.D. (2001). Analysis of relative gene expression data using real-time quantitative PCR and the 2(-Delta Delta C(T)) Method. *Methods* 25, 402–408. <https://doi.org/10.1006/meth.2001.1262>.

STAR★METHODS

KEY RESOURCES TABLE

REAGENT or RESOURCE	SOURCE	IDENTIFIER
<i>Antibodies</i>		
CD326 (EpCAM) Monoclonal Antibody (G8.8), FITC, eBioscience™	Invitrogen	Cat# 11-5791-82; RRID: AB_11151709
APC anti-mouse CD45 Antibody	Biolegend	Cat# 103112; RRID: AB_312977
Anti-mouse CD16/32 Antibody	Biolegend	Cat# 101302; RRID: AB_312801
Goat Anti-Mouse IgG Antibody (H+L), Biotinylated	Vector Laboratories	Cat# BP-9200; RRID: AB_2336171
Goat Anti-Rabbit IgG Antibody (H+L), Biotinylated	Vector Laboratories	Cat# BP-9100
HSP90 (C45G5) Rabbit mAb	Cell Signaling Technology	Cat# 4877; RRID: AB_2233307
Ki-67, Rabbit Monoclonal Antibody	Abcam	Cat# ab16667; RRID: AB_302459
Polyclonal Rabbit Anti-Cytokeratin, Wide Spectrum	Abcam	Cat# ab9377; RRID: AB_307222
TROMA III Cytokeratin 19	TROMA-III was deposited to the DSHB by Kemler, R. (DSHB Hybridoma Product TROMA-III)	Cat# ab-2133570; RRID: AB_2133570
Anti-Mouse IgG (H+L), HRP Conjugate	Sigma	Cat# 401253; RRID: AB_437779
Anti-Rabbit IgG (H+L), HRP Conjugate	Sigma	Cat# 401393; RRID: AB_437797
Goat anti-Mouse IgG (H+L) Cross-Adsorbed Secondary Antibody, Alexa Fluor 647	Invitrogen	Cat# A32728; RRID: AB_2633277
Goat anti-Rabbit IgG (H+L) Cross-Adsorbed Secondary Antibody, Alexa Fluor 488	Invitrogen	Cat# A-11008; RRID: AB_143165
Monoclonal Rabbit Phospho-S6 Ribosomal Protein (Ser235/236) antibody	Cell signaling	Cat# 4858; RRID: AB_916156
Polyclonal Rabbit Anti-Phospho-p70 S6 Kinase (Thr389) antibody	Cell signaling	Cat# 9205; RRID: AB_330944
Monoclonal Rabbit pS6 Ribosomal Protein antibody	Cell signaling	Cat# 2221
Polyclonal Rabbit Anti -p70 S6 Kinase antibody	Cell signaling	Cat # 9202; RRID: AB_331676
Monoclonal Rabbit Phospho-Akt (Ser473) antibody	Cell signaling	Cat# 4060; RRID: AB_2315049
Monoclonal Rabbit AKT (pan) antibody	Cell signaling	Cat# 4691; RRID: AB_915783
Monoclonal Mouse Anti-β-Tubulin antibody	Cell signaling	Cat# 3873S; RRID: AB_1904178
Monoclonal Rabbit Anti-β-Actin	Cell Signaling	Cat# 4970; RRID: AB_2223172
Monoclonal anti-β-Actin Antibody produced in mouse	Sigma	Cat# A2228; RRID: AB_476697
Monoclonal Mouse Anti KHK (B6)	Santa Cruz Biotechnology	Cat# sc-377411
Polyclonal Rabbit KHK C	SAB	Cat# 21709-2
Polyclonal Rabbit KHKA	SAB	Cat# 21708
Anti-KHK-A/C for immunohistochemistry	Sigma	Cat# HPA007040; RRID: AB_1079185
Monoclonal Rabbit Phospho-ERK (Thr202/Tyr204) antibody	Cell Signaling	Cat# 4370; RRID: AB_2315112
Monoclonal Rabbit ERK antibody	Cell Signaling	Cat# 4695s; RRID: AB_390779

(Continued on next page)

Continued

REAGENT or RESOURCE	SOURCE	IDENTIFIER
Monoclonal Rabbit GLUT5 antibody	Santa Cruz Biotechnology	Cat# sc-271055
Monoclonal Rabbit ALDOB antibody	Abcam	Cat# ab153828
Biological samples		
Human Paraffin Tissues	Biobank University Hospital Heidelberg	N/A
Mouse PDAC tissues	This paper	N/A
Chemicals and recombinant proteins		
ProLong™ Gold Antifade Mountant with DAPI	Invitrogen	Cat# P36931
ImmPACT® DAB Substrate, Peroxidase (HRP)	Vector laboratories	Cat# SK-4105; RRD: AB_2336520
Bovine Serum Albumin	Sigma-Aldrich	Cat#A2153
RIPA buffer (10X)	Cell Signaling Technology	Cat#9806
Phenylmethylsulfonyl Fluoride	Calbiochem	Cat# 329-9806
Mayer's Hematoxylin	Diapath	Cat# C0303
30% Acrylamide/Bis solution 29:1	Bio-Rad	Cat# 1610156
Hoechst 33342	Thermo Fischer Scientific	Cat# H3570
D-(+)-Glucose	Sigma	Cat# G8270
D-(-)-Fructose	Sigma	Cat# F0127
[14C (U)] D-fructose	Hartmann Analytic	Cat# ARC0116; RRD: SCR_015807
Sirius Red	Sigma	Cat# 36-554-8
TrypLE	Gibco	Cat# 12605-010
Collagenase from <i>Clostridium Hystoliticum</i> type V	Sigma	Cat# C9263
RNAlater Stabilization Solution	Thermo	Cat# AM7024
AdDMEM/F12	Life Technology	Cat# 12634-028
SILAC Advanced DMEM/F-12 Flex Media, no glucose	Thermo	Cat# A2494301
L-Arginine	Sigma	Cat# A5006
L-Lysine	Sigma	Cat# L5501
GlutaMAX Supplement	Life Technology	Cat# 35050-061
HEPES	Sigma	Cat# H4034
B27	Thermo	Cat# 17504044
N-2 Supplement	Life Technology	Cat# 17502-048
N-Acetyl-L-cysteine	Sigma	Cat# A9165
Nicotinamide	Sigma	Cat# N0636
Recovery Cell Culture Freezing Medium	Life Technology	Cat# 12648-010
TrypLE Select Enzyme	Life Technology	Cat# A12177-01
Matrigel	Corning	Cat# 356255
FGF10	Peptotech	Cat# 100-26
Recombinant Human EGF	Peptotech	Cat# AF-100-15
Gastrin I	Sigma	Cat# G9020
Recombinant Human EGF	Peptotech	Cat# AF-100-15
Recombinant Murine Noggin	Peptotech	Cat# 250-38
RSPO-1	Peptotech	Cat# 120-38
Collagenase IV	Sigma	Cat# C5138
DNase I Solution	Thermo Scientific	Cat# 90083

(Continued on next page)

Continued

REAGENT or RESOURCE	SOURCE	IDENTIFIER
HEPES (1M)	Gibco	Cat# 15630056
EdU (5-ethynyl-2'-deoxyuridine)	Life Technologies	Cat# A10044
Critical commercial assays		
High-Capacity cDNA Reverse Transcription Kit	ThermoFisher	Cat# 4368813
CellTiter-Glo® 3D Cell Viability Assay	Promega	Cat# G9681
Insulin ELISA	ALPCO	Cat# 80-INSRTU-E10-AL
PicoPure® RNA Isolation Kit	Invitrogen	Cat# KIT0204
KAPA SYBR FAST ABI	Roche	Cat# SFABIKB
Gateway LR Clonase II enzyme mix	Invitrogen	Cat# 11791-100
Gateway BP Clonase II enzyme mix	Invitrogen	Cat# 11789-020
EnzyChrom Fructose Assay Kit	Medibena	Cat# BA_EFRU-100
Rneasy Mini Kit	Qiagen	Cat# 74104
Nucleospin Tissue	MACHEREY-NAGEL	Cat# 740952.50
Click-iT Plus Alexa Fluor 647 Picolyl Azide Toolkit	Life Technology	Cat# C1064
jetPRIME®	Polyplus transfection	Cat# 114-07/712-60
Experimental models: Cell lines		
HEK293T	ATCC	Cat# CRL-11268
Human organoid lines	This paper	N/A
Mouse organoid lines	This paper	N/A
Mouse PDAC cell lines	This paper	N/A
Experimental models: Organisms/strains		
Ptf1atm1(cre)Hnak/RschJ	The Jackson Laboratory	RRID:IMSR_JAX:023329
B6.129P2-Trp53tm1Bm/J	The Jackson Laboratory	RRID:IMSR_JAX:008462
B6.129S4-Krastm4Tjy/J	The Jackson Laboratory	RRID:IMSR_JAX:008179
LSL-Kras ^{G12D/+} ; LSL-Trp53 ^{R172H/+}	Tyler Jacks Lab	N/A
LSL-Kras ^{G12D/+} ; LSL-Trp53 ^{R172H/+} ; Ptf1a-Cre (KPC ^{mut})	This paper	N/A
C57BL/6J-KhKctm1	Ozgene/ This Paper	N/A
C57BL/6J-KhKAtm1	Ozgene/ This Paper	N/A
KPC: LSL-KrasG12D/+;LSL-Trp53fl/+;Ptf1a-Cre	This paper	N/A
KPC-Khk-A ^{-/-} : LSL-KrasG12D/+;LSL-Trp53fl/+;Ptf1a-Cre-Khk-A ^{-/-}	This paper	N/A
KPC-Khk-C ^{-/-} : LSL-KrasG12D/+;LSL-Trp53fl/+;Ptf1a-Cre-Khk-C ^{-/-}	This paper	N/A
KPC-Khk-A/C ^{-/-} : LSL-KrasG12D/+;LSL-Trp53fl/+;Ptf1a-Cre-Khk-A/C ^{-/-}	This paper	N/A
Ptf1a-Cre-Khk-A ^{-/-}	This paper	N/A
Ptf1a-Cre-Khk-C ^{-/-}	This paper	N/A
Ptf1a-Cre-Khk-A/C ^{-/-}	This paper	N/A
Khk-A/C ^{-/-}	R. Johnson (University of Colorado)	N/A
Deposited data		
RNA-seq	This paper	

(Continued on next page)

Continued

REAGENT or RESOURCE	SOURCE	IDENTIFIER
<i>Oligonucleotides</i>		
Sh-RNA KhkA-1 Fwd	This paper, see Table S1	N/A
Sh-RNA KhkA-1 Rev	This paper, see Table S1	N/A
Sh-RNA KhkA-2 Fwd	This paper, see Table S1	N/A
Sh-RNA KhkA-2 Rev	This paper, see Table S1	N/A
Sh-RNA KhkC-1 Fwd	This paper, see Table S1	N/A
Sh-RNA KhkC-1 Rev	This paper, see Table S1	N/A
Sh-RNA KhkC-2 Fwd	This paper, see Table S1	N/A
Sh-RNA KhkC-2 Rev	This paper, see Table S1	N/A
<i>Oligonucleotides</i>		
<i>Hif1α</i> _Fwd	This paper, see Table S1	N/A
<i>Hif1α</i> _Rev	This paper, see Table S1	N/A
<i>KhkA/C</i> _Fwd	This paper, see Table S1	N/A
<i>KhkA/C</i> _Rev	This paper, see Table S1	N/A
<i>Khk-A</i> _Fwd	This paper, see Table S1	N/A
<i>Khk-A</i> _Rev	This paper, see Table S1	N/A
<i>Khk-C</i> _Fwd	This paper, see Table S1	N/A
<i>Khk-C</i> _Rev	This paper, see Table S1	N/A
<i>Slc2a1</i> _Fwd	This paper, see Table S1	N/A
<i>Slc2a1</i> _Rev	This paper, see Table S1	N/A
<i>Hk2</i> _Fwd	This paper, see Table S1	N/A
<i>Hk2</i> _Rev	This paper, see Table S1	N/A
<i>Aldob</i> _Fwd	This paper, see Table S1	N/A
<i>Aldob</i> _Rev	This paper, see Table S1	N/A
<i>Slc2a5</i> _Fwd	This paper, see Table S1	N/A
<i>Slc2a5</i> _Rev	This paper, see Table S1	N/A
β -actin_Fwd	This paper, see Table S1	N/A
β -actin_Rev	This paper, see Table S1	N/A
<i>Pdx1</i> _Fwd	This paper, see Table S1	N/A
<i>Pdx1</i> _Rev	This paper, see Table S1	N/A
<i>Ck19</i> _Fwd	This paper, see Table S1	N/A
<i>Ck19</i> _Rev	This paper, see Table S1	N/A
<i>Sox9</i> _Fwd	This paper, see Table S1	N/A
<i>Sox9</i> _Rev	This paper, see Table S1	N/A
<i>Hnf6</i> _Fwd	This paper, see Table S1	N/A
<i>Hnf6</i> _Rev	This paper, see Table S1	N/A
<i>Ptf1a</i> _Fwd	This paper, see Table S1	N/A
<i>Ptf1a</i> _Rev	This paper, see Table S1	N/A
<i>Cpa1</i> _Fwd	This paper, see Table S1	N/A
<i>Cpa1</i> _Rev	This paper, see Table S1	N/A
<i>Amy</i> _Fwd	This paper, see Table S1	N/A
<i>Amy</i> _Rev	This paper, see Table S1	N/A
<i>Ngn3</i> _Fwd	This paper, see Table S1	N/A
<i>Ngn3</i> _Rev	This paper, see Table S1	N/A
<i>Chga</i> _Fwd	This paper, see Table S1	N/A

(Continued on next page)

<i>Continued</i>		
REAGENT or RESOURCE	SOURCE	IDENTIFIER
Chga_Rev	This paper, see Table S1	N/A
Ins2_Fwd	This paper, see Table S1	N/A
Ins2_Rev	This paper, see Table S1	N/A
Klf4_Fwd	This paper, see Table S1	N/A
Klf4_Rev	This paper, see Table S1	N/A
Muc5ac_Fwd	This paper, see Table S1	N/A
Muc5ac_Rev	This paper, see Table S1	N/A
Muc6_Fwd	This paper, see Table S1	N/A
Muc6_Rev	This paper, see Table S1	N/A
Tff1_Fwd	This paper, see Table S1	N/A
Tff1_Rev	This paper, see Table S1	N/A
Slc2a2_Fwd	This paper, see Table S1	N/A
Slc2a2_Rev	This paper, see Table S1	N/A
Hk1_Fwd	This paper, see Table S1	N/A
Hk1_Rev	This paper, see Table S1	N/A
Myc_Fwd	This paper, see Table S1	N/A
Myc_Rev	This paper, see Table S1	N/A
Ldha_Fwd	This paper, see Table S1	N/A
Ldha_Rev	This paper, see Table S1	N/A
Got1_Fwd	This paper, see Table S1	N/A
Got1_Rev	This paper, see Table S1	N/A
Mdh2_Fwd	This paper, see Table S1	N/A
Mdh2_Rev	This paper, see Table S1	N/A
Pkm_Fwd	This paper, see Table S1	N/A
Pkm_Rev	This paper, see Table S1	N/A
Acly_Fwd	This paper, see Table S1	N/A
Acly_Rev	This paper, see Table S1	N/A
Cpt1a_Fwd	This paper, see Table S1	N/A
Cpt1a_Rev	This paper, see Table S1	N/A
Fasn_Fwd	This paper, see Table S1	N/A
Fasn_Rev	This paper, see Table S1	N/A
Acaca_Fwd	This paper, see Table S1	N/A
Acaca_Rev	This paper, see Table S1	N/A
Srebf1_Fwd	This paper, see Table S1	N/A
Srebf1_Rev	This paper, see Table S1	N/A
Srebf2_Fwd	This paper, see Table S1	N/A
Srebf2_Rev	This paper, see Table S1	N/A
Sqle_Fwd	This paper, see Table S1	N/A
Sqle_Rev	This paper, see Table S1	N/A
Acacb_Fwd	This paper, see Table S1	N/A
Acacb_Rev	This paper, see Table S1	N/A
Accs1_Fwd	This paper, see Table S1	N/A
Accs1_Rev	This paper, see Table S1	N/A
Accs2_Fwd	This paper, see Table S1	N/A
Accs2_Rev	This paper, see Table S1	N/A

(Continued on next page)

Continued

REAGENT or RESOURCE	SOURCE	IDENTIFIER
<i>Cycloph...</i> _Fwd	This paper, see Table S1	N/A
<i>Cycloph...</i> _Rev	This paper, see Table S1	N/A
18S_Fwd	This paper, see Table S1	N/A
18S_Rev	This paper, see Table S1	N/A
Recombinant DNA		
pET11a KHK-C	Aruna Asipu (Leeds, GB)	N/A
pET11a KHK-A	Aruna Asipu (Leeds, GB)	N/A
psPAX2	Addgene	Cat# 12260; RRID: Addgene_12260
pMD2.G	Addgene	Cat# 12259; RRID: Addgene_12259
pLKO.1 - TRC Cloning Vector	Addgene Plasmid	Cat#10878; RRID: Addgene_10878
Software and algorithms		
Aperio ImageScope	Leica (V 12.3.2.8013)	https://www.leicabiosystems.com/digital-pathology/manage/aperio-imagescope/ ; RRID: SCR_020993
Image J	Schneider et al., 2012	https://imagej.nih.gov/ij/ ; RRID: SCR_003070
GraphPad Prism	GraphPad software (V 8.4.2 (679))	https://www.graphpad.com/scientific-software/prism/ ; RRID: SCR_002798
Cell Ranger (3.1.0)	NA	https://support.10xgenomics.com/single-cell-gene-expression/software/pipelines/latest/what-is-cell-ranger ; RRID: SCR_017344
R v4.0.2	https://www.r-project.org/	NA
R package Seurat v3.2.0	https://satijalab.org/seurat/	RRID:SCR_016341
STAR v.2.5.1b	https://github.com/alexdobin/STAR	RRID:SCR_015899

RESOURCE AVAILABILITY

Lead contact

Further information and requests for resources and reagents should be directed and will be fulfilled by the lead contact, Markus Stoffel (stoffel@biol.ethz.ch).

Materials availability

Further information and requests for resources and reagents should be directed to and will be fulfilled by the [lead contact](#), Markus Stoffel (stoffel@biol.ethz.ch).

Data and code availability

ArrayExpress RNA-seq accession number: ArrayExpress: E-MTAB-12746.

No original code was generated in this study.

EXPERIMENTAL MODEL AND SUBJECT DETAILS

Mouse models

All mice were maintained under specific pathogen-free conditions a SPF animal facility at the ETH Phenomics Center (EPIC) at ETH Zürich. Maintenance and animal experiments were conducted in accordance with the Swiss Federal Veterinary Office (BVET) guidelines and approved by the local ethical committee, authorization numbers ZH018_15 and ZH055_17. *LSL-Kras^{G12D/+}* (Strain #:008179, LSL-K-ras G12D); *LSL-Trp53^{fl/+}* (Strain #008462, *p53^{LoxP}*; Ptf1a-Cre (Strain #023329, p48-cre) were obtained from Jackson Laboratory and crossed to obtain *KPC*. *LSL-Kras^{G12D/+}*; *LSL-Trp53^{R172H}* (KP), and *LSL-Kras^{G12D/+}*; *LSL-Trp53^{R172H/+}*; Ptf1a-Cre (*KPC^{mut}*) were obtained from Tyler Jack's (Howard Hughes Medical Institute). *KhkA/C^{-/-}* mice were

obtained from R. Johnson (University of Colorado). $KhkC^{lox/lox}$ and $KhkA^{lox/lox}$ were generated by Ozgene Pty Ltd (Bentley WA, Australia) using goGermline technology. Briefly, A 499bp region (chr5:31,084,234-31,084,732 mm39) encompassing exon 3c was flanked with loxP sites for $KhkC$, while a 384 bp region (chr5:31,083,850-31,084,233 mm39) encompassing exon 3a was flanked with loxP sites. The genomic 5' and 3' arms of homology and the floxed genomic region were generated by PCR amplification of C57BL/6 genomic DNA. The FRT-flanked neo cassette was inserted along with the 3' loxP site. Homologous recombination of the targeting vector was carried out by electroporation of C57BL/6 ES cell line and clones were selected for neomycin resistance. Correctly targeted ES clones were identified by Southern blot RFLP analysis and microinjected into goGermline blastocysts to generate germline chimeras.⁵¹ Male chimeric mice were obtained and crossed to C57BL/6J females to establish heterozygous germline offspring on pure C57BL/6 background. Following germline transmission, the *FRT-PGK-NeoR-FRT* cassette was deleted by mating to a transgenic line containing FLP recombinase. The *Flp* gene was removed by segregation in subsequent crosses. Pancreas-specific knockout of *KPC* transgenic mice were crossed with $KhkC^{lox/lox}$ and $KhkA^{lox/lox}$ mice to generate $KPC;KhkC^{-/-}$ and $KPC;KhkA^{-/-}$ mouse models. NSG mice were used for the xenograft PDAC models upon injection of pancreatic cancer cells derived from GEMMs. All mouse, except for the survival study, were euthanized at the age of 15 or 20 and 9 or 13 weeks for analysis.

Human sample collection

Paraffin-embedded pancreatic tissue from patients with PDAC and healthy controls were obtained from the Biobank (Pancobank) of the European Pancreas Center (EPZ), Department of General Surgery, Heidelberg University Hospital. All procedures were in compliance with the Ethics Committee of the medical faculty at the University of Heidelberg, Germany (Ethic vote No. S-708/2019) and the Helsinki Declaration. An informed consent was obtained from all patients. PDAC and donor samples were stained for KHK.

Pancreatic cancer cell culture

Cancer cells were derived from KPC , $KPC;KhkC^{-/-}$, $KPC;KhkA^{-/-}$, $KPC;KHK/C^{-/-}$ mouse tumors, sorted using Epcam+, CD45- strategy and were cultured in DMEM supplemented with 10% FBS and 1% penicillin/streptomycin (P/S). HEK-293T (human embryonic kidneys) cells were obtained from ATCC. Cells were cultured in DMEM supplemented with 10% FBS and 1% penicillin/streptomycin.

Human PDAC organoid culture

Human PDAC organoids were established from patients' surgical specimens and cultured as described in full detail by.⁵³ Human pancreatic tissue samples were provided by the Department of Pathology and Molecular Pathology, University Hospital Zurich, based on informed consent and study approval from the ethical committee (BASEC-Nr. 2017-01319). For all samples PDAC status was confirmed on corresponding tissue slides reviewed by board-certified pathologists. To establish organoid lines, tissue was chopped and digested in full medium containing collagenase type II (5 mg/ml). The digestion was stopped with advanced DMEM/F12 medium supplemented with HEPES (10 mM), Glutamax (1%) and P/S (1%). Cells were seeded as 20 μ l drop of Matrigel (Corning, growth factor reduced) into a 48-well suspension culture plate. Human PDAC organoids were cultured in Advanced DMEM supplemented with 1×10^{-4} M HEPES, 1x Glutamax, 1% Penicillin/Streptomycin, 1x B27, 1.25×10^{-3} M N-acetylcysteine, 50% Wnt3a conditioned medium (CM), 10% R-spondin-1 CM, 10% noggin CM, 1×10^{-4} M nicotinamide, 1×10^{-6} M prostaglandin E2, 50 ng mL⁻¹, EGF, 10×10^{-9} M gastrin, 100 ng mL⁻¹ FGF10 and 0.5×10^{-6} M A83-01.

Murine PDAC organoid culture

Pancreatic ducts were isolated from the whole organ of 20 weeks old KP, KPC , $KPC;KhkC^{-/-}$, $KPC;KhkA^{-/-}$, $KPC;KHK/C^{-/-}$ mice as previously described.⁵⁴ Each organoid line was isolated from an individual mouse. Isolated ducts organoids were embedded in growth-factor reduced (GFR)-Matrigel (Corning), and cultured in organoid medium (OM), which is composed of AddMEM/F12 (Gibco) supplemented with GlutaMAX (Gibco), HEPES (Gibco), Penicillin-Streptomycin (Invitrogen), B27 (Gibco), N-2 (Gibco), 1.25 mM N-Acetyl-L-cysteine (Sigma), 10 nM Gastrin I (Sigma) and the growth factors: 100 ng/ml FGF10 (Peprotech), 50 ng/ml EGF (Peprotech), 100 ng/ml Noggin, 100 ng/ml RSPO-1 (Peprotech), and 10 mM Nicotinamide (Sigma). For the first week after duct isolation the culture medium was supplemented with 100 μ g/ml Primocin (InvivoGen).

METHOD DETAILS

Organoid proliferation assays

Single cells were obtained by re-suspending organoids in medium through a fire-polished glass pipette, and then by enzymatic dissociation with TrypLE (Life Technologies). Cells (1500 cells per well) were embedded into growth factor-reduced Matrigel and seeded into a 96 well for incubation. Following 96 hours of culture, cell proliferation was determined by measuring cell viabilities (G9681, Promega) using the microplate reader (Tecan). Six replicate wells per condition were used. Luminescence data were analyzed with GraphPad Prism.

2D cell proliferation assay

For the proliferation assay, 1×10^5 cells/well were seeded in a 96-well plate and incubated for 72 h. Proliferation was monitored and analyzed by using Incucyte S3 *in vitro* system (Essenbioscience). Four pictures were recorded every 6 hrs for the 4 biological replicates and 6 technical replicates.

Migration assay

Migration assay was performed in 2D cancer cells derived from the four mouse genotypes by plating 3×10^5 cells per well of 96-well plate. Wound was performed using Incucyte Wound Maker and cell migration was monitored and analyzed by using Incucyte S3 *in vitro* system (Essenbioscience).

Plasmid constructions of over-expression and shRNAs knockdown of KhkA, KhkC and KhkA/C

The KHKA and KHKC overexpression plasmids were produced by sub cloning KHKA and KHKC from the pET11a-KHKA and pET11a-KHKC expression constructs (provided by A. Asipu) into the Gateway Entry vector pENTR1a and by LR-reaction in the pLenti-pgk-puro lentiviral expression vector. siRNAs targeting KhkA, KhkC or KhkA/C were designed using the Life Technologies BLOCK-iT RNAi Designer online tool (Life Technologies), searching for targets to KhkA, KhkC, KhkA/C transcripts. The TRC loop sequence CTCGAG was used. Two shRNAs were chosen as candidates for each isoform and cloned into the pLKO.1 lentiviral vector respectively. The presence of the shRNA was confirmed by sequencing (Micro-synth). ShRNAs were then tested in organoids for knockdown efficiency and specificity. Sh-KhkC, Sh-KhkA, Sh-KhkA/C sequences used in this study are listed in the Key Resource Table and [Table S1](#). A non-targeting shRNA vector SHC002 (Sigma) was used as a control.

Lentivirus production and transduction

Lentiviral particles were produced in HEK-293T cells that were purchased from American Type Culture Collection (ATCC). To prepare lentiviral particles, HEK-293T cells were transfected using JetPRIME® transfection reagents (JetPRIME®, Polyplus transfection, 114-07/712-60) as per the manufacturer's instructions. The virus in the supernatants from a 10 cm dish was concentrated by ultracentrifugation at 60,000g for 2 hrs at 4°C (Beckman). The viral concentrate was re-suspended in 50 µl PBS. Following dissociation of the organoids, the fragments were transduced with lentivirus by mixing with virus-containing medium in a 48-well plate. The mixture was then centrifuged at 600g for 1 h at room temperature and incubated for 6 h at 37°C. After spin down, the pellet was re-suspended in matrigel (Corning) and seeded 40 µl into a 24-well plate. The plate was incubated at 37°C for 5 to 15 min until the basement matrix was solidified and then adding the culture medium. Selection was performed by adding puromycin (1 µg/ml) to the medium.

Insulin Elisa assay

To determine mouse serum insulin levels, blood was obtained from the tail vein and centrifuged for serum separation. Insulin was measured by Insulin ELISA Kit (ALPCO, 80-INSRTU-E10-AL) following the instructions.

Glucose measurement

Blood glucose values were measured with a Bayer Contour XT glucometer after 6 h of fasting at the endpoint of the treatment.

Immunohistochemistry (IHC) and immunofluorescence (IF)

For both IHC and IF tissue sections were processed as follows: deparaffinizing, unmasking, pre-staining, blocking and secondary stainings. Deparaffinization was performed using six-step procedure of alcohol scale 5mins each. The slides were drained off the excess solution and were then immersed in ionized water for 5 min. Further, unmasking or antigen retrieval procedure was followed which involved immersing the section slides in solution pH 6 (Citrate, Company: Diapath, Cat No. T0050) in the microwave at 98°C for 25 min. The slides were allowed to cool at room temperature for 25 min. The section slides were washed with 1xPBST (0.5% Tween20), twice for 3 min each, followed by staining procedure. Only for IHC but not for IF, blocking procedure began by incubating the slides with 3% H₂O₂ for 10 min, and followed by 1xPBST washes as before and performing protein block. For both IHC and IF, protein blocking was performed using Protein-Block solution (DAKO Agilent technologies, Cat No. X0909) for 10 min at room temperature. When antibodies were developed in mice, the tissues were blocked for mouse cross-reactivity using a biotinylated anti-mouse antibody (Vector Laboratories, Cat No. BP-9200). Sections were stained with respective primary antibodies at room temperature for 1 h followed by 3 washes with 1xPBST as before. These slides were further incubated with respective secondary antibodies, for IHC, anti-Mouse (Vector Laboratories, Cat No. BP-9200), anti-Rabbit (Vector Laboratories, Cat No. BP-9100) and for IF using aluminum foil to protect from light, Fluor chrome antibodies (conjugated with either with Alexa- 488, -647). In both cases, secondary antibodies were diluted at 1:200 in 1xPBS solution for 30 min at room temperature. For IF, upon completion of secondary antibody incubation procedure, slides were washed 3 times with 1xPBST with minimum exposure to light and upon draining out the PBST, slides were incubated with mounting media with DAPI (Invitrogen, P36931) ready to be visualized under a fluorescent confocal microscope. For IHC, during secondary antibody incubation, Vectastain ABC solution was prepared (Company: Vector laboratories, Cat No. PK-6100) at the dilution of 1:150 of both Solution A and Solution B in 1xPBS solution followed by 30 min incubation at room temperature. Upon completion of secondary antibody stainings, slides were washed for 3 times with 1xPBST followed by ABC solution staining for 30 min at room temperature. After ABC, slides were washed 3 times with 1xPBST and final steps of IHC stainings were performed. DAB staining was performed using DAB solution (Company: Vector laboratories, Cat No. SK-4105. One drop of Chromogen in 1ml of Diluent solution) and allowed to stain for no more than 2-3 min at room temperature. Immediately slides were washed 3 times with 1x PBST and counter staining was performed using hematoxylin solution (Diapath, C0303). At the end of IHC staining, sections were dehydrated using deparaffinization procedure after which slides were mounted with coverslip using mounting media (Sigma, 03989). The Sirius red staining was performed using a solution of Picro-sirius red (0.5 g) and saturated aqueous solution of picric acid (500 ml) in de-waxed and hydrated paraffin sections for 1 h followed by two washing steps with acidified water (5 ml acetic acid glacial to 1 liter of distilled water), the dehydrate in three changes of 100% ethanol, clear in xylene and mount.

Normal, tumor tissue samples were fixed in 10% neutral-buffered formalin overnight. Tissues were washed thoroughly under running tap water followed by processing using ethanol and embedded in paraffin according to standard protocols. Sections (3 µm) were prepared for antibody detection. Slides were prepared as consecutive sections. Human PDAC and donor section used was provided by the PancoBank of the European Pancreas Center Heidelberg and used in accordance with the regulations of the biobank and the vote of the ethics committee of the University of Heidelberg.

Ketohexokinase activity assay

The ketohexokinase activity assay was modified by adding Protease Inhibitor Cocktail (Roche) and PhosSTOP (Roche) to the reaction mixture.¹⁹ The reaction was performed at 37°C for 2 h after adding 140 µg protein for each reaction. The remaining fructose was measured using a Spectra MAX 190 plate reader (Molecular Devices). Reactions without protein were used as negative controls, and lysate from KHK-C overexpression cells was used as a positive control.

Lysis

- Lysis Buffer (1 ml): 800µL water, 50 µl 1M Imidazol buffer pH 7, 150 µl KCl, 0.5 M
- Lyse 10 wells of organoids in 100 µl Lysis Buffer or 100 mg tissue in 1 ml lysis buffer.
- Sonication: 10 to 15 pulses, 40% amplitude
- Centrifugation: 15 min at 15,500 g, 4°C

- Determine protein concentration with BCA kit

Preparation of reaction mixture

- Prepare 0.1 M D-Fructose solution fresh (e.g. 180 µg Fructose in 10 mL water)
- For one reaction in a volume of 100 µl, add in this order:
 - 0.9 µl 0.1 M D-Fructose
 - 8 µl 0.5 M NaATP
 - 0.8 µl MgCl₂
 - 20 µl 5 M KAc
- Mix by pipetting up and down several times
- 8 µl 0.5 M NaF
- 10 µl 0.2 M N-Acetylglucosamine
- 5 µl 1 M Imidazole Buffer pH 7
- up to µl 100 H₂O
- Include T0 samples without protein (or with protein but without ATP and Mg) and a blank (no fructose and ATP)

Reaction

- Add 140 µg protein to reaction mixture
- Incubate 2 h at 37°C in a heating block
- Stop reaction by the addition of 50 µl ZnSO₄ (1 M) and 250 µl Ba(OH)₂ (0.1 M)
- Centrifuge 15 min at 5500 g
- Take off supernatant

Seliwanoff reaction

- Use 100 µl of the supernatant
- Add 100 µl 0.1% alcoholic resorcinol
- Add 300 µl 30% HCl
- 8 mins at 80°C in a water bath at 37°C
- Let cool down at RT
- Measure duplicates in a 96 well plate (200 µl/well): absorbance at 515 nm.

[¹⁴C (U)] D-fructose incorporation into DNA and protein *in vitro*

Three lines of organoids for each condition were seeded in a 24-well plate and cultured in the complete medium. After 2 days, fresh medium containing 1 µCi/ml [¹⁴C (U)] D-fructose (Hartmann Analytic) was added and incubated overnight. Then, organoids were washed three times with PBS and proteins were extracted as described in Western blot section. Genomic DNA was extracted using a kit according to manufacturers' instructions (MACHEREY-NAGEL, 740952.50). Radioactivity was measured in a Beckman LS6500 scintillation counter (Beckman) and normalized to the amount of DNA or protein.

Western blot

Mouse pancreatic tumor samples or organoids were lysed using 1x RIPA buffer (Cell signaling, 9806) supplemented with Phenylmethanesulfonyl fluoride (PMSF; Millipore Sigma, catalog 329-98-6) and incubated on ice for 20 min. Samples were centrifuged at 14'000 rpm for 20 min. Protein concentration was determined by the BCA kit (Thermo Fisher 23227). Equal amounts of protein were subjected to SDS-polyacrylamide gel electrophoresis (SDS-PAGE), 10% based on the molecular weight of the proteins of interest and

transferred on to 0.45 μm nitrocellulose membrane (Perkin Elmer, NBA083C001EA). After protein transfer, membranes were blocked in 5% milk solution and membranes were probed with the indicated antibodies overnight at 4°C. The membranes were incubated with horseradish peroxidase-conjugated (HRP-linked) secondary antibodies anti-rabbit IgG (Sigma, 401393, 1:5000) or anti-mouse IgG (Sigma, 401253, 1:5000) and developed using enhanced chemoluminescence (ECL) substrate. Membranes were exposed to Fusion Solo S imaging system (Vilber). Blots were semi-quantitatively analyzed by densitometry using ImageJ 1.52 v (National Institutes of Health). Primary antibody against were used at the following concentration: KHKA/C (1:500, Santa Cruz), KHKC (1:500, SAB), KHKA (1:500, SAB), p-ERK (1:1000, CST), ERK (1:1000, CST), p-AKT (1:1000), AKT (1:1000, CST), GLUT5 (1:500, Santa Cruz), Aldolase B (1:1000, Abcam), Phospho-p70 S6K (1:1000, CST), Phospho-S6 (Ser235/236) (1:1000, CST) p70 S6K (1:1000, CST), pS6 (1:1000, CST) .

Antibodies

Primary and secondary antibodies were used at the concentrations indicated in the Key Resources Table according to manufacturer's instructions.

EdU incorporation assays

EdU incorporation-based proliferation assay was performed with KPC organoids. Briefly, 10 μM EdU (Life Technology, C10643) was added to the organoid cultures and pulsed for 4 h. Subsequently, organoids were recovered from matrigel and were dissociated into single cells by TrypLE (Gibco) and mechanical mean using a fire-polished glass Pasteur pipette. Cells were fixed with 4% paraformaldehyde (PFA) in PBS for 10 min at 4°C. PFA was removed and cells were twice washed with PBS. After permeabilizing the cells in PBS containing 0.2% Triton-X100 (PBS-T) for 15 min at 4°C, the "click-iTEdU" reaction was carried out using the Click-iT Plus EdU Alexa Fluor 647 Picolyl Azide Toolkit (Life Technology, C10643) according to the manufacturer's instructions. Cells were then resuspended in 500 μl PBS and subjected to FACS analysis (BD LSRFortessa; BDFACSDiva software). EdU incorporation imaging was performed as described above without any dissociation of the organoids. The stained organoids were imaged under confocal microscopy (Leica).

Real-time PCR analysis

RNA from organoids was isolated with the RNeasy Mini Kit (Qiagen) and reverse-transcribed to cDNA (Applied Biosystems) according to the manufacturer's instructions. RNA from pancreata was isolated by immediately immersing the dissected tissue into RNAlater and cutting into small pieces. After homogenized by freeze slamming with Trizol and centrifugation, the supernatant was transferred into a 2 ml tube followed by spinning with chloroform. The upper aqueous layer was used for the RNA extraction with the RNeasy Mini Kit. First-strand cDNA was synthesized with random hexamer primers using the High-Capacity RNA-to-cDNA Kit (No. 4368813; Applied Biosystems).

Quantitative real-time PCR reactions were carried out with 2x KAPA SYBR FAST qPCR Mastermix (No. KK4601; KAPA Biosystems) and run on a Light Cycler 480 (Roche). Ct values were normalized to the house-keeping genes beta-actin, 18S rRNA or cyclophilin (Ppia). The sequences of primers used in this study are listed in the [Table S1](#). Expression levels were calculated using the $2^{-\Delta\Delta\text{CT}}$ method⁵⁵

Fructose or glucose feeding

25% of fructose (Sigma, F0127) was dissolved in tap water. The solution was filtered using a filter bottle (Millian SA, 99500). Fructose feeding experiments started when mice were at the age of 10 weeks. The water was refreshed every 5 days.

Analysis of metabolites in cancer cell lines

5×10^5 cancer cells from all four mouse genotypes were plated in 10 cm dish in DMEM 10% FBS 3 mM glucose and 10 mM of fructose. After 48 h, the growth medium was removed from the plate and the cells were washed with AMBIC (ammonium bicarbonate) buffer at room temperature. 400 μl of 80% ice cold MeOH were added to the plate and cells were detached from surface by scraping gently. The procedure was repeated a second time, to complete the cell harvesting, and the cell suspensions obtained in the two harvesting rounds were pooled in a single sample. Sample homogenization and metabolite extraction has been achieved by freeze-thaw-cycle lysis. The tubes containing the cell suspension were placed in liquid N₂ for 2 min, followed by 5 min incubation at room temperature in a shaker (600 rpm). Such cycle was repeated

4 times, followed by vortexing/mixing by pipetting and transfer a fixed volume of suspension to a new test tube. The metabolite enriched supernatant was separated from the cell debris by centrifugation at 10,000 g for 10 min at 4°C after a 15 min incubation of the cell suspension on ice. The pellet was kept for protein quantification and the results of such quantification were used to normalize the concentration of the metabolites extracts.

Sample preparation for LC-MS analysis and LC-MS analysis

100 mL methanol extracts were dried under nitrogen stream, reconstituted in 20 µl water (MS grade) plus injection buffer (90% ACN, 8.8% MeOH, 50 mM ammonium acetate, pH 7.0). The solution was vortexed and centrifuged at 16,000 x g, 4°C for 15 min. 50 ml of the supernatant were transferred to a glass vial with narrowed bottom (Total Recovery Vials, Waters) for LC-MS injection. In addition, method blanks, QC standards, and pooled samples were prepared in the same way to serve as quality control for the measurements.

Metabolites were separated on a nanoAcquity UPLC (Waters) equipped with a BEH Amide capillary column (150 mm x 130 mm, 1.7 mm particle size, Waters), applying a gradient of 5 mM ammonium acetate in water (A) and 5 mM ammonium acetate in 95% acetonitrile (B) from 90% B to 50% B over 10 min, followed by 2 min at 98% B and 4 min re-equilibration at 90% B. The injection volume was 1 ml. The flow rate was adjusted over the gradient from 3 to 2 ml/min. The UPLC was coupled to Synapt G2Si mass spectrometer (Waters) by a nanoESI source. MS1 (molecular ion) and MS2 (fragment) data were acquired using negative polarization and MS^E over a mass range of 50 to 1200 m/z at MS1 and MS2 resolution of >20,000.

Untargeted metabolomics data analysis

Metabolomics data sets were evaluated in an untargeted fashion with Progenesis Q1 software (Nonlinear Dynamics), which aligns the ion intensity maps based on a reference data set, followed by a peak picking on an aggregated ion intensity map. Detected ions were identified based on accurate mass, detected adduct patterns and isotope patterns by comparing with entries in the HMDB Data Base. A mass accuracy tolerance of 5 mDa was set for the searches. Fragmentation patterns were considered for the identifications of metabolites. All biological samples were analyzed at least in triplicate and quality controls were run on pooled samples and reference compound mixtures to determine technical accuracy and stability.

Illumina RNA sequencing

Pancreatic tumors from all four genotypes mouse models were resected and processed for single cell suspension followed by RNA sequencing and analysis using the following procedure:

-Single cell suspension: PDAC tumors were isolated, minced and processed for single cell suspension. Tissues were digested in 2 ml of Digestion Buffer composed by Collagenase IV 3% in RPMI, 10% FBS + 1% Pen/Strep, DNase I 30 U/µl, Hepes 10 mM. The cell suspension was incubated for 30 min at 37°C on a rocker. Then, the digestion was stopped adding 1 ml of RPMI 10% FBS + 1% P/S. The cells suspension was filtered through a 100 µm cell strainer and kept on ice for 4 min. Then cells suspension was filtered again through a 40 µm cell strainer and spun down at 1500 rpm for 5 min at 4°C. FACS staining was performed using the following antibodies: anti-Epcam-FITC and anti-CD45-APC and the Epcam⁺; CD45⁻ cells were sorted for total RNA extraction using PicoPure® RNA Isolation Kit (Invitrogen, KIT0204).

The quantity and quality of the isolated RNA was determined with a Fragment Analyzer (Agilent, Waldbronn, Germany). Due to the low RIN number of some samples the SMARTer Stranded Total RNA-Seq Kit - Pico Input Mammalian (Clontech Laboratories, Inc., A Takara Bio Company, California, USA) was used in the succeeding steps. Briefly, total RNA samples (0.25–10 ng) were reverse-transcribed using random priming into double-stranded cDNA in the presence of a template switch oligo (TSO). When the reverse transcriptase reaches the 5' end of the RNA fragment, the enzyme's terminal transferase activity adds non-templated nucleotides to the 3' end of the cDNA. The TSO pairs with the added non-templated nucleotide, enabling the reverse transcriptase to continue replicating to the end of the oligonucleotide. This results in a cDNA fragment that contains sequences derived from the random priming oligo and the TSO. PCR amplification using primers binding to these sequences can now be performed. The PCR adds full-length Illumina adapters, including dual barcodes for multiplexing. Ribosomal cDNA is cleaved by ZapR in the presence of the mammalian-specific R-Probes. Remaining fragments are enriched with a second round of PCR amplification using primers designed to match Illumina adapters. The quality and quantity of the enriched libraries were validated using the Fragment Analyzer (Agilent, Waldbronn,

Germany). The product is a smear with an average fragment size of approximately 360 bp. The libraries were normalized to 10 nM in Tris-Cl 10 mM, pH 8.5 with 0.1% Tween 20. The equimolar pool of samples was spiked into a NovaSeq6000 run targeting 200×10^6 reads on a S1 FlowCell (Novaseq S1 Reagent Kit, 100 cycles, Illumina, Inc, California, USA).

RNA seq data analysis

The quality of the sequencing reads was assessed utilizing FastQC (version 0.11.9). Alignment of total RNA (stranded) to the reference mouse genome (M27) was carried out using STAR (version 2.7.9a) in a two-pass mode. Gene expression was quantified at the gene level through the use of comprehensive annotations provided by Gencode (vM27 GTF File). Samples were normalized for library size and transformed using the variance stabilizing transformation in R statistical environment with the DESeq2 (version 1.38.1) pipeline. In the differential expression analysis between groups, an Independent Filtering procedure was employed to exclude genes that were not significantly expressed in the majority of samples under consideration. Unless specified, all gene set enrichment analyses were performed using the Limma (version 3.54.0) package. Gene sets were obtained from the Molecular Signature Database (MSigDB) and Reactome. Multiple testing correction was applied to P-values using the false discovery rate (FDR) with a significance threshold of 0.05.

QUANTIFICATION AND STATISTICAL ANALYSIS

All experiments were performed on biological replicates as mentioned in the respective figure legends. Sample size for each experimental group/condition is reported in the appropriate figure legends. All data points are presented for quantitative data, with an overlay of the mean with SEM. Statistically significant differences between control and experimental groups were determined using Multiple Student's t-tests (two-tailed, unpaired), one-way ANOVA with Sidák's and Tukey multiple comparison difference tests, and log-rank (Mantel-Cox) test as indicated in the appropriate figure legend and text. Significances are indicated as * $P < 0.05$, ** $p < 0.01$ and *** $p < 0.001$, and **** $p < 0.0001$. All statistical analyses were performed using GraphPad Prism 9, Microsoft Excel 2016 or R-Studio.